remote sensing

MDPI

Article

Reconstruction of a Monthly 1 km NDVI Time Series Product in China Using Random Forest Methodology

Mengmeng Sun [1,2], Adu Gong [1,2,*], Xiang Zhao [1,2], Naijing Liu [1,2], Longping Si [1,2] and Siqing Zhao [1,2]

1 State Key Laboratory of Remote Sensing Science, Jointly Sponsored by Beijing Normal University and Aerospace Information Research Institute of Chinese Academy of Sciences, Faculty of Geographical Science, Beijing Normal University, Beijing 100875, China; smm2021@mail.bnu.edu.cn (M.S.); zhaoxiang@bnu.edu.cn (X.Z.); liunj@mail.bnu.edu.cn (N.L.); silongp@bnu.edu.cn (L.S.); zhaosiqing@mail.bnu.edu.cn (S.Z.)

2 Beijing Engineering Research Center for Global Land Remote Sensing Products, Institute of Remote Sensing Science and Engineering, Faculty of Geographical Science, Beijing Normal University, Beijing 100875, China

* Correspondence: gad@bnu.edu.cn; Tel.: +86-010-58806178

Abstract: The normalized difference vegetation index (NDVI) is one of the most common metrics used to describe vegetation dynamics. Unfortunately, low-quality pixels resulting from contamination (by features including clouds, snow, aerosols, and mixed factors) have impeded NDVI products' widespread application. Researchers have thought of several ways to improve NDVI quality when contamination occurs. However, most of these algorithms are based on the noise-negative deviation principle, which aligns low-value NDVI products to an upper line but ignores cases where absolute surface values are low. Consequently, to fill in these research gaps, in this article, we use the random forest model to produce a set of high-quality NDVI products to represent actual surface characteristics more accurately and naturally. Climate and geographical products are used as model inputs to describe environmental factors. They represent the random forest (RF) model that establishes relationships between MODIS NDVI products and meteorological products in high-quality areas. In addition, auxiliary data and empirical knowledge are employed to meet filling requirements. Notably, the random forest (RF) algorithm exhibits a mean absolute error (MAE) of 0.024 and a root mean squared error (RMSE) of 0.034, in addition to a coefficient of determination (R^2) value of 0.974. Furthermore, the MAE and RMSE of the RF-based method decreased by 0.014 and 0.019, respectively, when compared to those of the STSG (spatial–temporal Savitzky–Golay) plan and by 0.013 and 0.015, respectively, when compared to the LSTM (long short-term memory) method. R^2 increased by 0.039 and 0.027, respectively, compared to the STSG and LSTM methods. We introduced a novel series of NDVI products that demonstrated consistent spatial and temporal connectivity. The novel product exhibits enhanced adaptability to intricate environmental conditions and promises the potential for utilization in investigating vegetation dynamics within the Chinese region.

Keywords: MODIS NDVI time series product; contaminated areas; random forest; reconstruction

check for updates

Citation: Sun, M.; Gong, A.; Zhao, X.; Liu, N.; Si, L.; Zhao, S. Reconstruction of a Monthly 1 km NDVI Time Series Product in China Using Random Forest Methodology. *Remote Sens.* **2023**, *15*, 3353. https://doi.org/10.3390/rs15133353

Academic Editors: Gintautas Mozgeris and Sébastien Gadal

Received: 18 April 2023
Revised: 25 June 2023
Accepted: 28 June 2023
Published: 30 June 2023

1. Introduction

The use of NDVI is widespread due to its simplicity and stability and its close correlation with and high sensitivity to vegetation greenness. More specifically, NDVI reduces certain types of band-correlated noise (noise related positively) and the effects of changes in direct and diffuse irradiance, clouds and cloud shadows, sun and view angles, topography, atmospheric correction, and other factors. Rationalization can also minimize calibration and instrument-related errors to a certain extent. The time at which rationing can reduce noise depends on the noise correlation between red and NIR responses. In addition, it depends on responses as to the degree to which the surface exhibits Lambertian (angle-independent) behavior [1,2]. MODIS NDVI time series products have become widespread in monitoring vegetation growth in the face of global change. Through the quantitative analysis of the

NDVI, changes in vegetation growth patterns can be accurately discerned and observed over time. Such monitoring provides valuable information about global change processes and their impact on vegetation growth [3–5]. Nevertheless, specific pixels contaminated by clouds, snow, aerosols, and other compounding factors are found in these products, thereby precluding their practical application. As a result, the presence of the factors above can compromise the efficacy of these products. These factors can ultimately diminish their overall suitability for usage. Although preprocessing steps such as using a maximum value composite can remove some noise, a considerable amount remains in MODIS NDVI time series products [6]. Therefore, developing an efficient reconstruction method for postprocessing and obtaining high-quality NDVI time series products is necessary to remove the noise that the preprocessing steps cannot clearly achieve [7–9].

Previous studies have proposed reconstruction methods based on three principles for NDVI noise reduction: filter-based, temporal, and hybrid. First, many methods have used filters to fill the gaps caused by contaminated areas, such as the Savitzky–Golay filter and the mean value iterative filter [10–12]. Second, the temporal method is based on a mathematical function that aims to fit the daytime growth curve, such as the asymmetric Gaussian or double logistic part [13,14]. Temporal methods usually entirely use the relationship between vegetation phenology and long time series products to reduce the noise deviation on the time series curve. These curves are of the same category and standard libraries [15–17]. Third, the hybrid method considers temporal continuity and spatial correlation to correct long-term data gaps, such as the material–spatial iteration method and the spatiotemporal tensor method [18,19]. In addition, Cao et al. introduced a technique for reducing noise that incorporates spatiotemporal information with the SG filter, called spatial–temporal Savitzky–Golay (STSG) [20]. The results showed that STSG performed significantly better than the four previously widely used methods (i.e., the asymmetric Gaussian, double logistic, Fourier-based, and Savitzky–Golay filter). One obvious advantage was that STSG addressed the problem of continuous NDVI gaps. STSG effectively increased local low NDVI values and avoided overcorrecting common NDVI values during crop harvest. The long short-term memory network (LSTM) is a specific type of recurrent neural network (RNN) that has been modified to enhance its performance in time series prediction [21]. The unique neuron structure of LSTM selectively remembers information and converges on the optimal solution more efficiently than traditional RNNs. The LSTM achieves this through several controllable gates (namely the forgetting gate, input gate, and output gate) that facilitate the passage of information between different units within the hidden layer. Although these methods follow other principles, they all obey one rule. This mechanism enables the extraction of temporal features from time series data, creating a prediction model capable of accurately predicting long-term trends. A reconstructed NDVI product can correct for noise by iteratively updating deviations from the time series curve of the noisy point. The angle from the standard library is compared to the one in the same category [21,22].

While these existing methods have been widely used to reconstruct low-quality NDVI areas, two challenges still need to be addressed. The first challenge is filling in the remaining gaps (e.g., temporally determined and continuous spatial–temporal gaps) in the MODIS NDVI time series due to cloud and snow conditions. To solve this problem, the interpolation method is usually used [23]. However, how to fill in continuous gaps or sudden changes in the time series is yet to be discovered. Therefore, finding a robust method to estimate missing values more accurately is critical [12]. The second challenge is identifying the noise level, which may indicate over-alignment [24]. Many machine learning (ML) methods have been used to produce high-quality NDVI products [25–27]; however, these methods need to pay more attention to the unique periodic characteristics of multiyear accumulations. Several attempts have been made to address their gaps, e.g., applying hundreds of time series images to reconstruct the long-term NDVI products [17,19,28] to obtain a smooth curve that ignores short-term changes based on vegetation growth.

Despite the efforts regarding the method mentioned earlier, the NDVI products were primarily reconstructed without considering the impact of temperature, rainfall, and other information on the vegetation growth process in the MODIS NDVI time series product [18,29–31]. Therefore, finding a more stable gap-filling method that can effectively determine how to process low NDVI values, for example, whether to maintain or directly correct common NDVI values before processing them, is imperative. Considering this gap, we describe a novel technique to reconstruct NDVI products in contaminated areas in the present article. This technique was developed by making spatial and temporal features, continuous multiyear time series data, and multiple products [32]. This method can be used to reconstruct NDVI products using multisource quantitative remote sensing products, like FAPAR and LAI, as well as factors related to vegetation growth, like longitude, latitude, and elevation. This is carried out to avoid the effect of NDVI products alone when several low-quality products are in a row. This study reconstructed NDVI data from low-quality regions using the random forest (RF) method, environmental factors, and historical data from remote sensing products. This led to spatiotemporal continuous monthly average NDVI products. The product can monitor vegetation growth, ecological change, and species evolution.

The rest of this article is structured as follows: Section 2 covers the data sources. Section 3 describes the algorithm and process in detail. Section 4 presents the model's performance results and a comparison with those of other products. Sections 5 and 6 discuss and conclude.

2. Study Area and Datasets

2.1. Study Area

China is a vast country with 34 administrative regions covering 9.6 million square kilometers. The research region considered in this study spans from longitude 73°40′ to 135°2′E and latitude 3°52′ to 53°33′N and encompasses extensive grasslands, agricultural land, and woodland. The eastern region of China has more cultivated and forested land than the western region, mainly green and desert. Due to its geographical location, China experiences many climate conditions. These include moderate continental climates in the north, northeast, and south and highland mountain climates in the Tibetan Plateau. The northwest region is arid and semi-arid, while the southeast region is semi-humid and humid. Moreover, China's elevation and precipitation levels divide the country into eight subregions, each with unique climatic conditions.

2.2. Datasets

This study used several products as input data, and post reconstruction NDVI products were exported as output products. Table 1 lists the input product data sources. Nine products in the Global Land Surface Satellite (GLASS) product series were u in NDVI reconstruction, including albedo products [33], such as Albedo BSA VIS, Albedo WSA NIR, Albedo WSA SWIR, and Albedo WSA VIS, evapotranspiration (ET) [34], photosynthetically active radiation absorbed fraction (FAPAR) [35], fractional vegetation cover (FVC) [36], gross primary production (GPP) [37], and leaf area index (LAI) [38]. The meteorological products used in this study were the product of temperature and precipitation, which were derived from a dataset with a monthly temporal resolution and $0.5° \times 0.625°$ spatial resolution called the Modern-Era Retrospective Analysis for Research and Applications version 2 (MERRA-2) reanalysis [39]. In addition, the product was available from 1982 to 2015. Obtaining precise surface elevation information for remote sensing information retrieval was imperative. Therefore, we also considered using NASA DEM in this study for reconstructing NDVI, which was developed for long-range postprocessing for the Topographic Radar Mission [40].

Table 1. The introduction of the products used in this study.

Data	Spatial Resolution	Time Resolution	Data Source
NDVI	1 km	Monthly	MOD13A3
Albedo (BSA VIS/WSA NIR/WSA SWIR/WSA VIS)	1 km	Eight days	GLASS
ET	1 km	Eight days	GLASS
FAPAR	1 km	Eight days	GLASS
FVC	1 km	Eight days	GLASS
GPP	1 km	Eight days	GLASS
LAI	1 km	Eight days	GLASS
Precipitation	0.5°	Monthly	MERRA2
Temperature	0.5°	Monthly	MERRA2
DEM	30 m		NASADEM
Longitude	1 km		According to the longitude range of China
Latitude	1 km		According to the latitude range of China

3. Methodology

Reconstructing high-quality MODIS NDVI products is quite challenging due to continuous missing areas. Due to the influence of clouds, snow, and aerosols on the NDVI product, there are some temporal and spatial series gaps. More sophisticated processing methods are required to improve MODIS NDVI time series products. Based on the combination of NDVI acquisition methods and their correlation with other products, we considered using multiple products to extract NDVI to complete the repair and filling tasks.

The proposed method was to generate continuous, long-span products with a monthly temporal resolution and a 1 km spatial resolution from 2001 to 2015. In addition, the high-quality areas in MOD13A3 were used as a reference to evaluate the performance of the proposed method. The quality flag layer illustrates the reliability of MODIS NDVI time series products and determines whether a value is good or contaminated by clouds, snow, ice, etc. It indicates that RI = 0 represents good NDVI quality, RI = 1 means some uncertainty in the NDVI, and multiple RI values indicate contaminated area pixels. The machine learning method divides datasets into training, validation, and testing. The training set is used to train the machine learning model. This involves the machine learning algorithm learning from the dataset and adjusting its parameters to arrive at the most effective predictive model. Through training the model on the training set, it can discern patterns and connections within the dataset. This ultimately facilitates its ability to accurately predict outcomes from unfamiliar data.

The model's parameters are adjusted using the validation set to optimize its performance during training. The selection of hyperparameters, such as the number of layers or decision tree depth, is required when training a neural network. The model's performance is evaluated on a validation set with varying parameter settings to identify the most effective ones that prevent overfitting. Overfitting occurs when the model performs exceptionally well on training data but needs to improve on new, unobserved data. The final step in evaluating model performance is using a distinct testing set. This comprises data that the model still needs to observe. The model's performance on unseen data can be assessed by making predictions on this testing set and comparing the predicted and actual labels. Such an evaluation plays a crucial role in determining the model's generalization ability, demonstrating its proficiency in processing novel data.

To summarize, the process of constructing a machine learning model involves the utilization of a training set for model training. In addition, there is a validation set for parameter adjustment to prevent overfitting and a testing set for model performance evaluation. We can develop high-performance machine learning models and robust generalization capabilities by adequately partitioning the datasets.

The flowchart of this paper is shown in Figure 1. Initially, gathering pertinent information required for the investigation, including ecological commodities, meteorological data, and geographical data, was imperative. Subsequently, the data needed to undergo various procedures such as format conversion, scaling, resampling, clipping, and synthesis of monthly average data (averaging data every eight days a month). Incorporating MOD13A3 long and short bit rules, the second step involved the selection of high-quality samples that met the specified requirements for a given month. Additionally, combining the pieces from every 12 months yielded high-quality samples for the entire year. To ensure representativeness, a specific number of high-quality models were randomly and uniformly selected for each category across various provinces in China, covering the period from 2001 to 2015. In the third step of the process, model parameters were established for training based on the samples created in step 2. Machine learning models, LSTM and RF, were trained. In the fourth step, LSTM, STSG, and RF algorithms were evaluated using verification data. The R^2 and RMSE of high-quality MOD13A3 were used for comparison purposes. Afterward, the trained model was used with the data to forecast the low-quality region. Finally, the model's projection results for the low-quality areas were employed to fill in the original low-quality-region data, resulting in a time series dataset of superior quality.

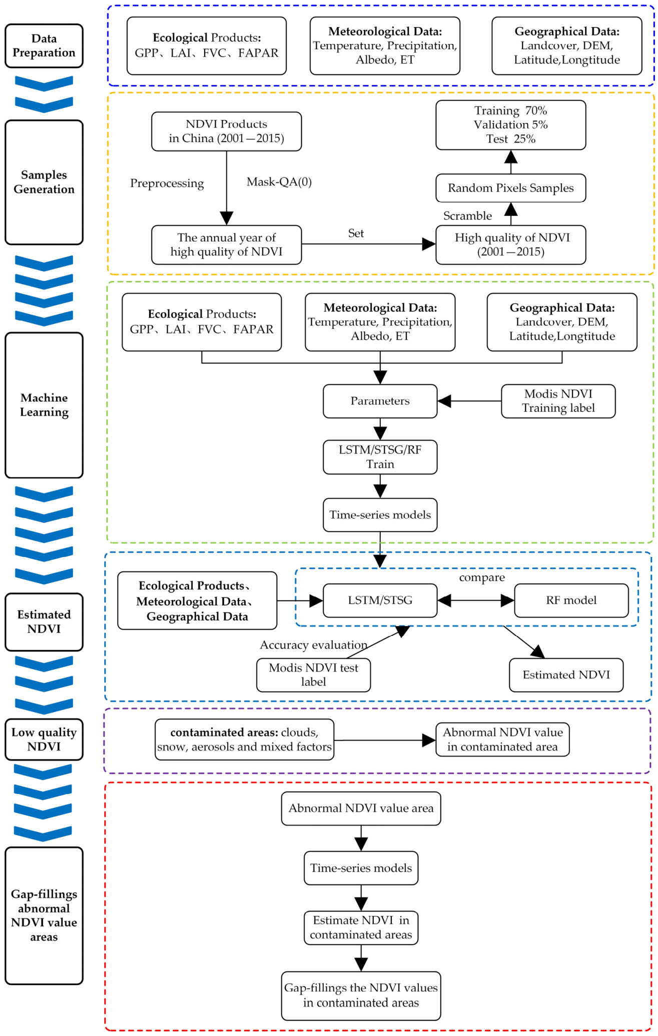

Figure 1. The flowchart of the proposed estimation method for the MODIS NDVI product in the contaminated areas of China. RF, LSTM, and STSG abbreviations represent random forest, long short-term memory, and the spatiotemporal Savitzky–Golay filter.

We thoroughly analyzed and examined the problems from two perspectives. In addition, we used spatial distribution images and histograms to illustrate MODIS NDVI quality. Figure 2a shows the spatial distribution of low- and high-quality products caused by clouds, snow, aerosols, and mixed factors. We found that high-quality samples were mainly concentrated in the central and northwestern regions, while low-quality areas due to aerosols, clouds, and snow were primarily located in the south and northwest. This distribution pattern was aligned with the area's industrial development and essential meteorological conditions site.

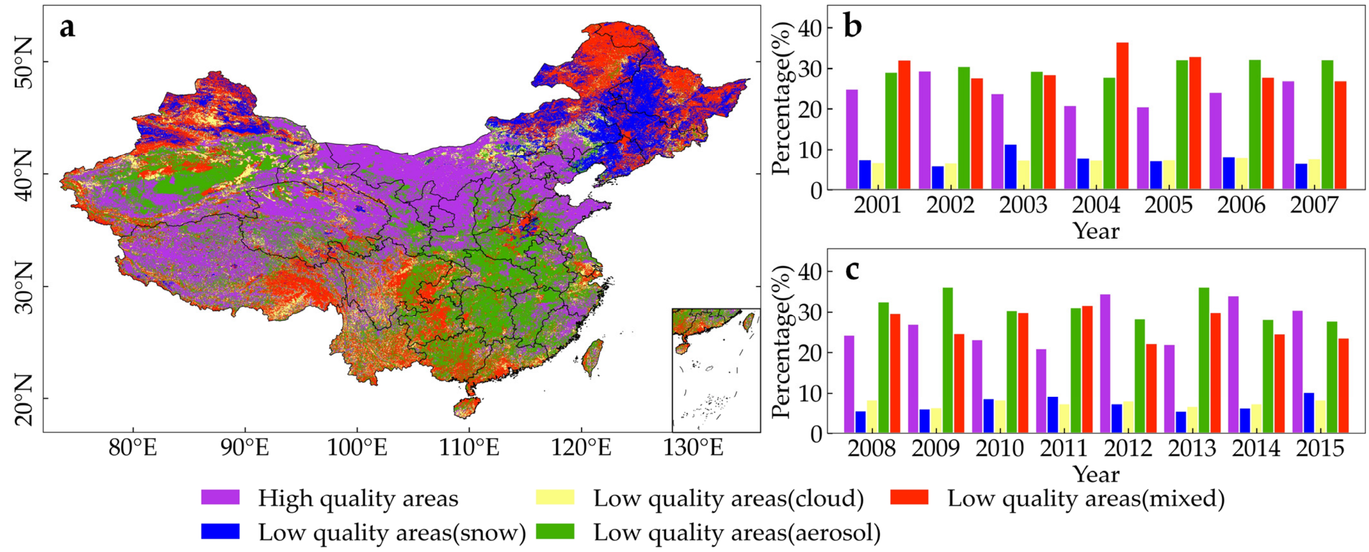

Figure 2. The spatial distribution maps and bar graphs of low-quality areas in China from 2001 to 2015 are based on the quality assurance (QA) of MODIS NDVI products. (**a**) illustrates the spatial distribution of pollutant factors, namely snow, cloud, aerosol, and mixed elements. (**b**) presents the annual percentage of incidents in various regions from 2001 to 2007. (**c**) displays the rates for different areas from 2008 to 2015.

To systematically analyze the distribution of NDVI products, we presented the results as simple statistical proportions. Our approach included using a histogram to objectively describe and understand the spatial distribution of NDVI products (Figure 2b,c). Clouds, snow, aerosols, and various factors caused low-quality areas. Multiple factors, such as clouds, snow, aerosols, and mixed factors, caused various factors in low-quality areas. Snow contributed to a relatively small proportion of low-quality NDVI. In contrast, clouds, aerosols, and a combination of factors contributed to a large proportion. MODIS NDVI time series products had many contaminated areas, resulting in gaps and limited applications. Adverse weather conditions and cloud cover caused decreased lower NDVI values in contaminated sites. Reconstructing high-quality MODIS NDVI time series data and developing research methods to repair gaps in contaminated regions remain challenging. Investigating suitable methods for reconstructing NDVI products and generating continuous spatial and temporal NDVI product series is essential.

3.1. Data Preprocessing

Initially, creating a time series was necessary to consolidate the conversion rate, resampling, clipping, and monthly average data synthesis. "Upscaling" refers to increasing an image's size while decreasing its spatial resolution. We utilised three rounds of convolution to transform NASA's Digital Elevation Model (NASA DEM) from a 30 m scale to a 1 km scale. Standard interpolation methods include a nearest neighbour, bilinear, and cubic convolution techniques to scale images. Among these, cubic convolution interpolation represents a more advanced approach. This algorithm performs linear interpolation using 16 neighbouring grayscale values around the target sample point. This method produces superior results by considering both the direct grayscale influence of the four adjacent points and the rate at which grayscale values change among neighbouring points. Although bicubic interpolation imposes a significant computational burden, it represents the best approach to image scaling. Therefore, we used an ascending scale with three convolutions to adjust the resolution from high to low. This was to convert a 30 m NASA DEM to a 1 km DEM with three interpolations.

In the second phase, high-quality samples were created by synthesising data and selecting areas based on NDVI product distribution. This resulted in a sample set that satisfied the model requirements. From 2001 to 2015, sample insertion and concatenation were performed, and the NDVI product was prioritised as label data.

3.2. Training Samples from High-Quality Areas of MODIS NDVI in China

Owing to the constraints imposed by the prevailing climate conditions and geographical location, the dataset employed for the model training fell short of good diversity. Diversity would have meant encompassing all of the climatic zones across the globe. Moreover, some areas needed more samples to be improved. Additionally, some land samples exhibited low numbers and their distribution focused on specific regions. For instance, forests dominated coastal regions. At the same time, other areas were scarce while the other parts were limited, leading to a need for more meaningful characteristic learning. As a result, it is imperative to delve deeper into developing algorithms that facilitate sample balancing and land classification to enhance estimates' precision.

Faced with the above problems, this paper adopted some strategies. For the first time, we relied on quality control documentation when initially evaluating high-quality samples. Then, based on this documentation, the pieces needed to meet a QA value of 0 or 1 for the short rule and a QA of 6–7 (aerosol), which should be 00, 01, 10, and 14–15 (clouds, snow). Secondly, to address the problem of unbalanced samples, which may have led to the overfitting of models with a large proportion, we selected samples based on the categorised products. We set a fixed percentage for selecting other categories in the respective states. This enabled us to address the challenges posed by overfitting and ensure that our samples were representative and diverse.

As illustrated in Figure 3, each province exhibited unique distribution and category characteristics. Fortunately, the samples met the criteria for balanced treatment conditions in China, covering a broad range of categories, quantities, and geographical features. Our selected samples were evenly distributed across their respective provinces, representing the overall population. Furthermore, we recommend employing a more sophisticated algorithm to learn the linear relationship between MODIS NDVI and estimated NDVI. This enhanced the accuracy and reliability of our findings, leading to more robust results.

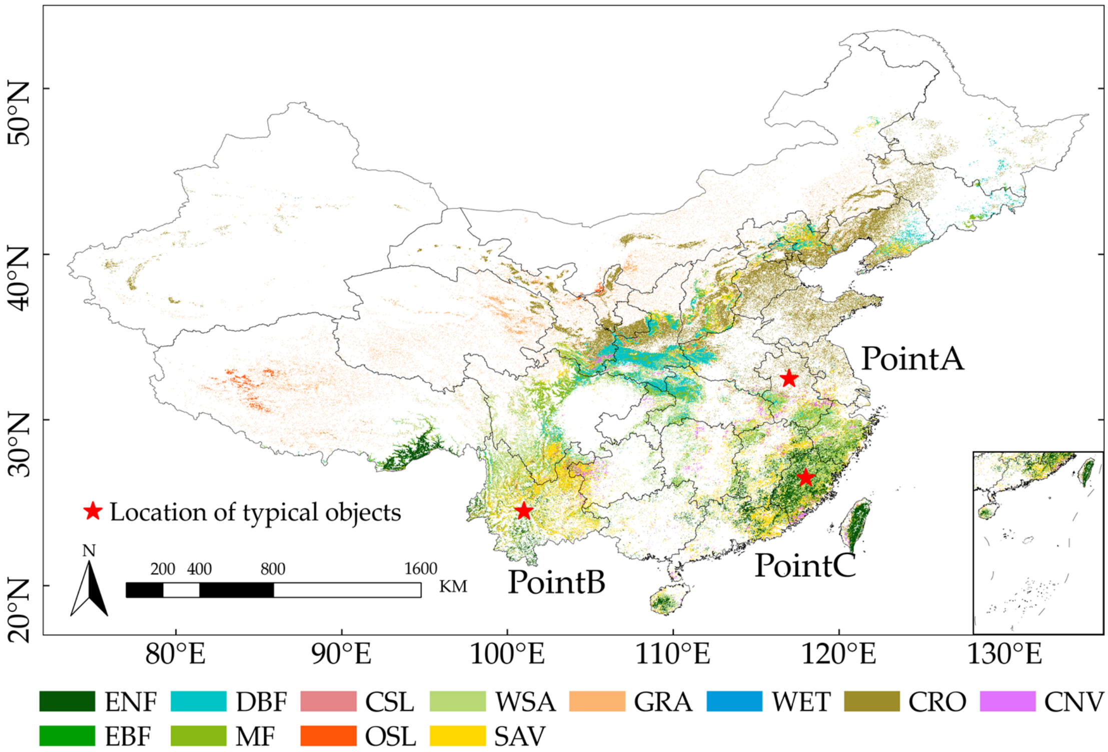

Figure 3. High-quality sample distribution map for 2001–2015. ENF presents evergreen needleleaf forest; EBF: evergreen broadleaf forest; DBF: deciduous broadleaf forest; MF: mixed forest; CSL: closed shrubland; OSL: open shrubland; WSA: woody savanna; SAV: savanna; GRA: grassland; WET: permanent wetland; CRO: cropland; CNV: cropland/natural vegetation mosaic.

3.3. Reconstruction Models

3.3.1. RF Model and Optional Parameters

RF is a continuous value prediction algorithm based on multiple decision trees, which can solve regression problems [41,42] and be applied to supervised classification [43–45]. It requires using bootstrap samples to generate multiple sub-training datasets, then using decision trees to fit each dataset, and finally taking the average of the prediction results of numerous decision trees [43]. In addition, the number of decision trees was based on the distribution of the samples via voting or averaging, which determined the method's performance [46]. Specifically, the rule reliability was also based on the splitting number, and the splitting numbers were based on the Gini index positively associated with rule reliability, which is relatively complex. Specifically, there are 12 products in this paper, taking place over 15 years. The year requires a significant workload, requiring a multiprocessing approach to handle it. Based on the above reasons, we used a default set of decision trees and (300, 4), which is an empirical location used by many researchers [42,43,46].

In the study, we constructed the relationship between the predicted value and the response variables to estimate the NDVI value. We used two main steps, the learning model acquisition phase and gap-filling in the contaminated areas of the MODIS NDVI time series product (Figure 1), to deal with these problems. The acquisition of training models primarily involved generating training samples, determining the generation of training samples, and choosing the optimal model. The trained model can be developed with high-quality sample illustrations and be a reference for forecasting contaminated areas. A high-quality place was obtained based on quality control documents during the sample acquisition stage. The proportion of samples in each category was fixed according to a principle that ensured that the samples were dispersed across provinces. The optimal model acquisition stage obtained a stable model based on the training samples and then selected the optimal training model based on the validation and test samples. The filling phase of the contaminated area mainly included obtaining low-quality data areas and estimating and filling the NDVI values of the regions. The NDVI of the infected areas was inputted into the optimal model, and the raw NDVI values in the contaminated areas were replaced with the estimated NDVI values. Moreover, we selected the estimated NDVI based on quantitative and qualitative evaluation results.

3.3.2. LSTM Model and Optional Parameters

Because the long short-term memory network (LSTM) can control the forgetting and updating gate, it can minimize the escalation, disappearance, or expansion during training. Therefore, it has many applications and excellent performance in natural language processing, speech recognition, and time sequence prediction [47–49]. Moreover, it has robust long-term dependency capabilities and can process sequential products [21,50].

In this study, we developed a five-layer deep neural network model for estimating NDVI, including an input layer, two LSTM layers, a dense layer, and an output layer. Specifically, the number of samples was N, and the number of time steps was 12. Our method's batch size was m, which increased the calculation speed. Moreover, the most effective performance was determined to be obtained with a batch size of 64. A dropout mechanism was introduced to the dense layer to prevent overfitting, and the dropout rates were empirically fixed at 0.5. As a result, the performance of the LSTM model was evaluated by utilizing two LSTM layers with 50 and 30 hidden units, respectively. Moreover, some parameters existed, such as Adam, a gradient-descending-based optimizer, and a learning rate of 0.001.

3.3.3. STSG Model and Optional Parameters

The STSG algorithm principle is a time-sequence-based approach used to fill the missing value in the MODIS NDVI time series product [20]. Currently, it exploits time sequence similarities between the same pixel class and spatial correlations between different types for long-term correction in the interval data gaps. The NDVI time sequence for a specific pixel was estimated based on the NDVI values observed in the neighbor pixels. Thus, NDVI calculations may give essential previous knowledge about the NDVI growth trajectory of the target pixel. In addition, we updated the NDVI time series by concatenating the original NDVI estimates with the pixel's raw NDVI time series. Subsequently, we calculated the weights of each NDVI in this updated time series and used a weighted SG filter to smooth the NDVI time series.

To validate the proposed RF method, we conducted a simulation experiment comparing LSTM and STSG and evaluated their performance through statistical histogram and spatial pattern comparisons. Furthermore, we tested the ability of the RF-based method to capture local phenological features for harvesting in the Taiwan cultivated area (TCA) in the North China Plain. This area consists of double-cropped croplands and broad-leaved deciduous forests, resulting in complex NDVI profiles throughout the year, making it a suitable case for comparing different reconstruction models. We verified whether the RF-based method could outperform the LSTM and STSG methods by retaining low NDVI actual values, while successfully simulating the harvest characteristics. Two methods were used to conduct the comparison of different NDVI reconstruction products. The first method compared the reconstructed NDVI with high-quality data across China's entire high-quality NDVI area. With the second method, the long-term robustness of the products was assessed under different climate conditions from 2001 to 2015. We used RMSE, R^2, MAE, and bias to evaluate the performance of the models. We also examined the high-quality-area MAE, the spatial distribution chart of RMSE, and the year-on-year change trend to determine whether the product had real phenology.

Finally, we found that NDVI reconstruction was necessary for cloudy areas to minimize missing data and reduce the negative impact of poor atmospheric conditions on NDVI values, which was crucial for addressing the effects of climate change. To enhance the reliability of our study, we used 15 years of products for the visual assessment of various vegetation types to determine general vegetation characteristics. We preserved high-quality NDVI values and substituted contaminated values with reconstructed NDVI values. We compared the performance of the RF, LSTM, and STSG models in correcting the contaminated pixels. To investigate phenological characteristics, we focused on mixed forests in the Yunnan, Fujian, and Chongqing provinces.

4. Results

4.1. Product Intercomparison

A comparison of the original NDVI products and reconstructed products generated using the STSG, LSTM, and RF models is presented in Figure 4. The RF and LSTM predictions exhibited high R^2 values, and most data points were clustered tightly around y = x. The NDVI output from the RF-based model displayed the highest accuracy among the models. The RF-based model yielded the highest R^2 value (0.965) and the lowest RMSE (0.0428) and MAE (0.0291) values for high-quality areas, indicating its superior performance in comparison to the LSTM and STSG methods. Consequently, the RF model was considered to be the most effective technique for reconstructing NDVI products.

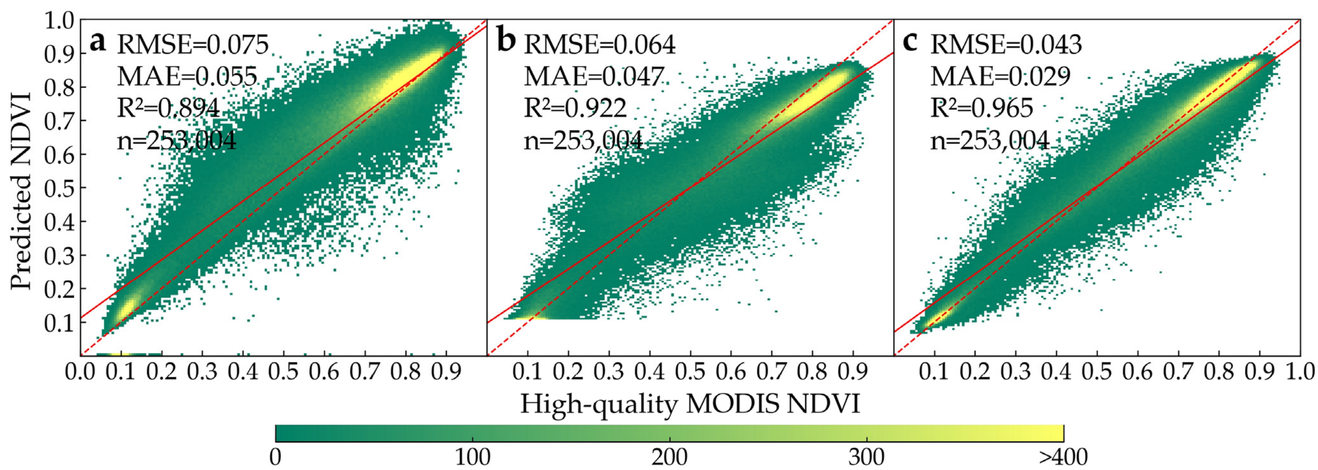

Figure 4. The comparative analysis of NDVI estimates using various methods in June, based on pixels in high-quality areas. The three methods used in the study were short-term satellite imagery gap-filling (STSG), long short-term memory (LSTM), and random forest (RF), as shown in panels (**a**), (**b**), and (**c**), respectively. Note: The red solid line depicts the forecast line, while the red dashed line represents the 1:1 line.

The results of the reconstruction of the long-time series curves in high-quality regions in China from 2001 to 2015 are presented in Figure 5. Statistical comparison outcomes such as relative RMSE, R^2, MAE, and relative bias are highlighted in the figure. The study findings indicated that the RF-based method generated more accurate and precise results for these high-quality areas. This discovery is significant, as it implies that the RF-based approach outperformed the STSG and LSTM methods regarding its ruggedness and adaptability in consistently reconstituting NDVI.

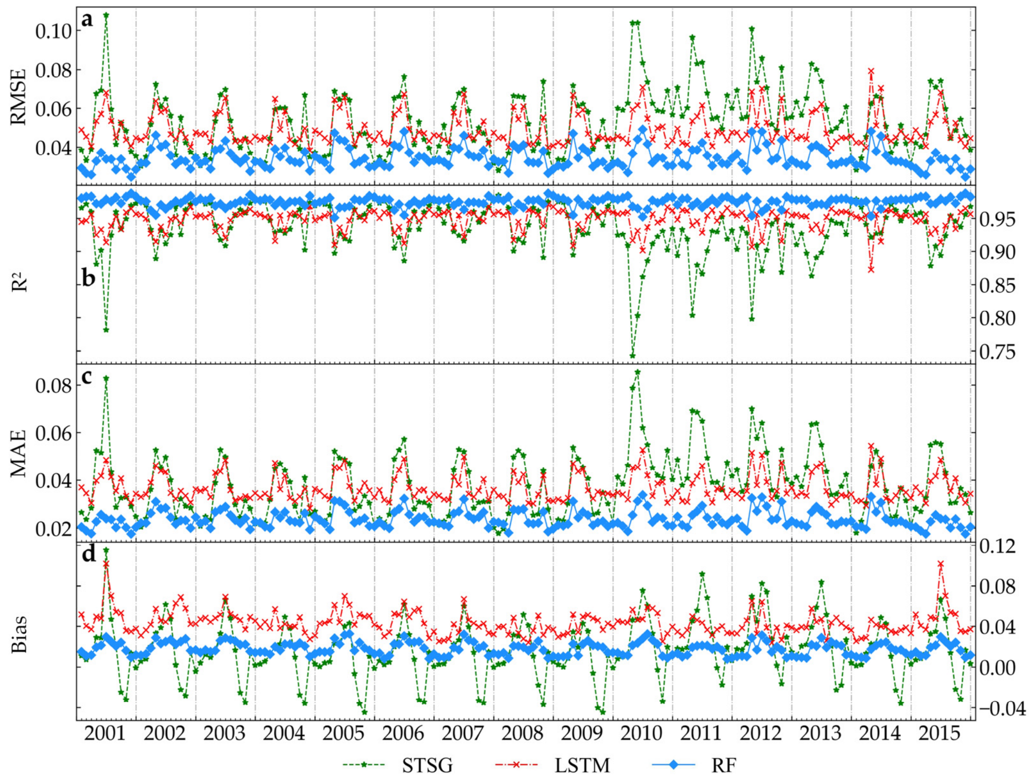

Figure 5. The comparisons of different methods based on the seasonal characteristics of NDVI in high-quality areas from 2001 to 2015. Comparison of the other methods based on seasonal factors of NDVI in high-quality regions during 2001–2015. The four indexes used in the analysis were RMSE, R^2, MAE, and bias comparisons of monthly NDVI estimation, as shown in panels (**a**–**d**), respectively.

A comparison of methods for estimating MODIS NDVI using quantitative and qualitative approaches is presented in Figure 6. Lower values of RMSE and MAE suggest greater accuracy in reconstruction performance. The findings indicated that the RF model was the most effective, with mean RMSE and MAE values of 0.034 and 0.026, respectively, on a national scale. Regarding spatial distribution, areas with an RMSE and MAE below 0.032 accounted for over 50% and 70% of the total area, respectively. The RF reconstruction result exhibited exceptional performance in locations such as the Inner Mongolia Plateau, Sichuan Basin, Loess Plateau, North China Plain, Southeast Coast, eastern Yunnan–Guizhou Plateau, and northern Qinghai–Tibet. However, some local regions, such as the Northern Plains and coastal areas, had RMSEs and MAEs greater than 0.064 due to various crop varieties and insufficient samples of corresponding vegetation types. Last, limitations intrinsic to the study include inadequate characterization and forest concentration in coastal areas.

The observations depicted in Figure 7 delineate the changes in China's high-quality areas in the past 15 years. Linear regression adjustment lines were utilized in this study to detail the trends in vegetation change. Notably, the post reconstruction NDVI, derived from different approaches, exhibited consistent trends. Since 2007, the NDVI values have demonstrated a general increase. This indicates an increase in vegetation and an overall improvement in the ecological environment in China.

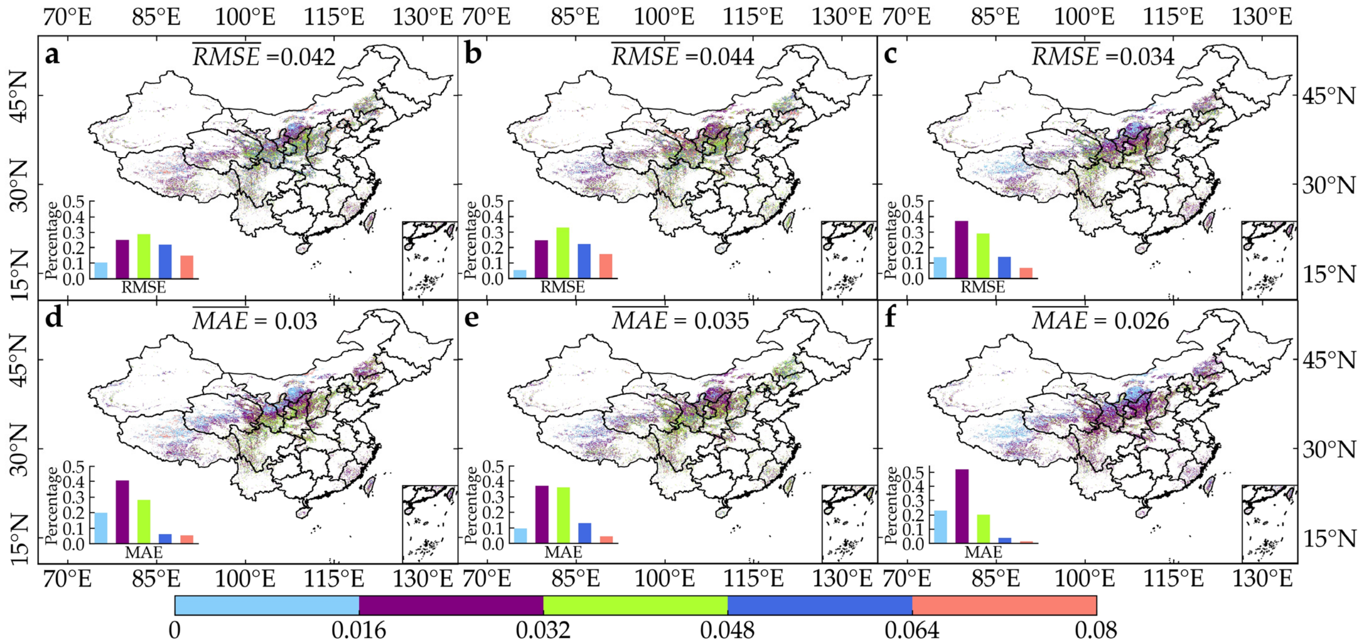

Figure 6. The performance of the reconstruction methods, namely STSG, LSTM, and RF, in high-quality areas. The evaluation was conducted by calculating the average root mean square error (RMSE) and mean absolute error (MAE) between the reconstructed normalized difference vegetation index (NDVI) and the reference NDVI for all pixels. The inset in each panel provides a bar graph depicting the percentage distributions of RMSE and MAE. Note: Quantitative assessments were based on the average of RMSE (shown at (**a**) STSG; (**b**) LSTM; (**c**) RF); and MAE between the reconstructed NDVI and the reference NDVI for high-quality pixels (shown at (**d**) STSG; (**e**) LSTM; (**f**) RF).

4.2. The Comparison of Biome Categories

The reconstructive process using RF alone is depicted in Figure 8. The figure shows that the raw product displayed noticeable spatially continuous gaps due to numerous inherent factors, such as rain, clouds, aerosols, and other impediments (left). The corrected figure represents using the estimated NDVI to fill in the low-quality values in the original NDVI. The ensuing reconstructed NDVI significantly improved the product's overall quality by mitigating the limitations caused by these factors. The reference curve embodies the average normalized difference vegetation index (NDVI) curve pertinent to a specific category within a selected province, for instance, Fujian Province. This reference curve is a product of meticulously chosen high-quality samples, whereby the selection of which is contingent on the quality assurance (QA) file quality identification bits. This QA file serves as a critical tool in ensuring the reliability and validity of the data used, thereby enhancing the accuracy of the resulting NDVI curve. It is paramount to highlight that these high-quality samples hold across all twelve months of the year. This implies that the reference curve, and hence the average NDVI curve, maintain their relevance and applicability throughout the year, providing a consistent and reliable measure of vegetation for the specified category within the chosen province.

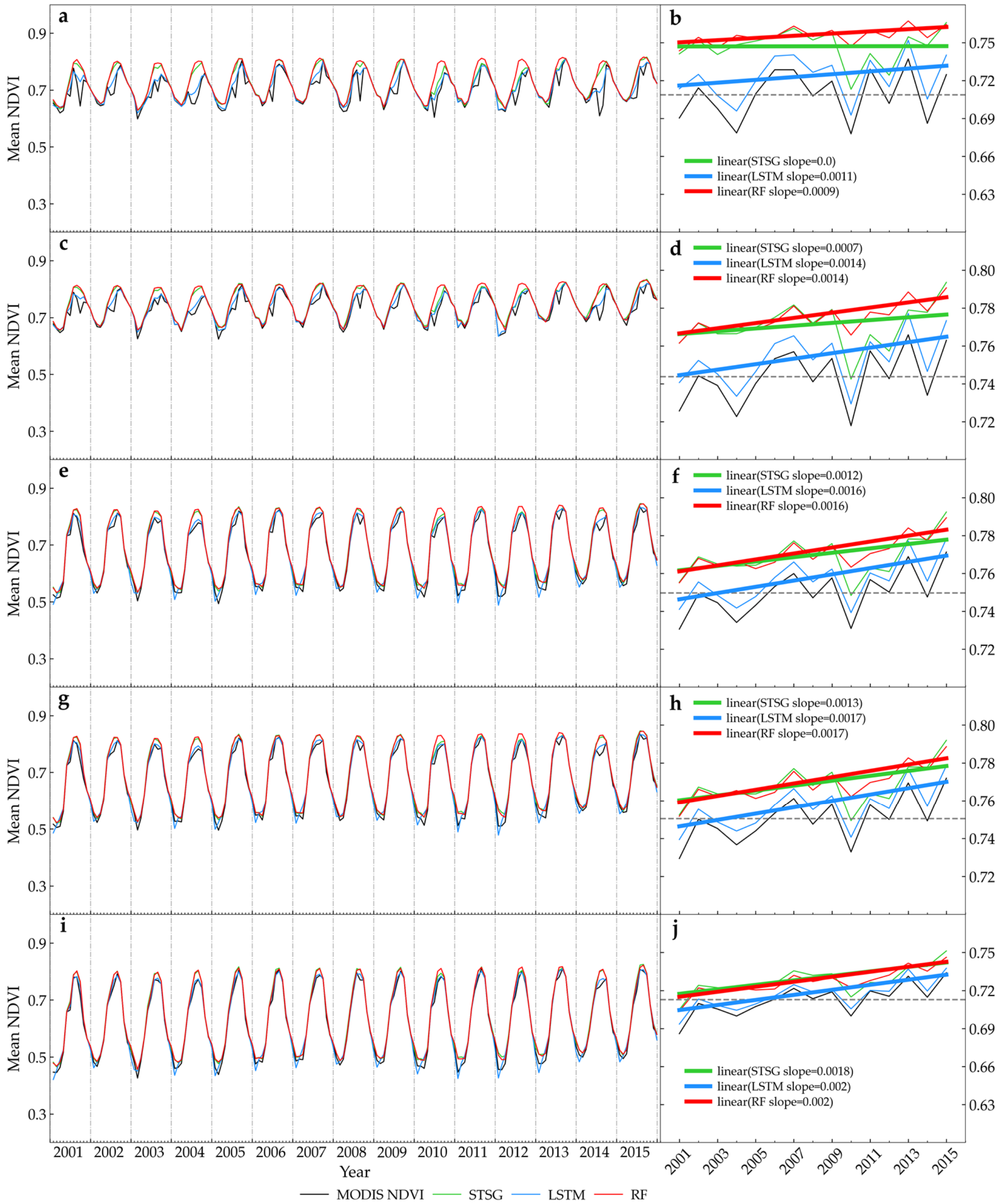

Figure 7. The NDVI trends in high-quality regions of China from 2001 to 2015. The time series of typical characteristics of the points affected by clouds, snow, aerosols, and mixed factors are represented by (**a**,**c**,**e**,**g**,**i**); the comparison of the time series between the original MODIS NDVI product and the estimated NDVI product in 2015 for evergreen needleleaf forests, evergreen broadleaf forests, and mixed forests are represented by (**b**,**d**,**f**,**h**,**j**).

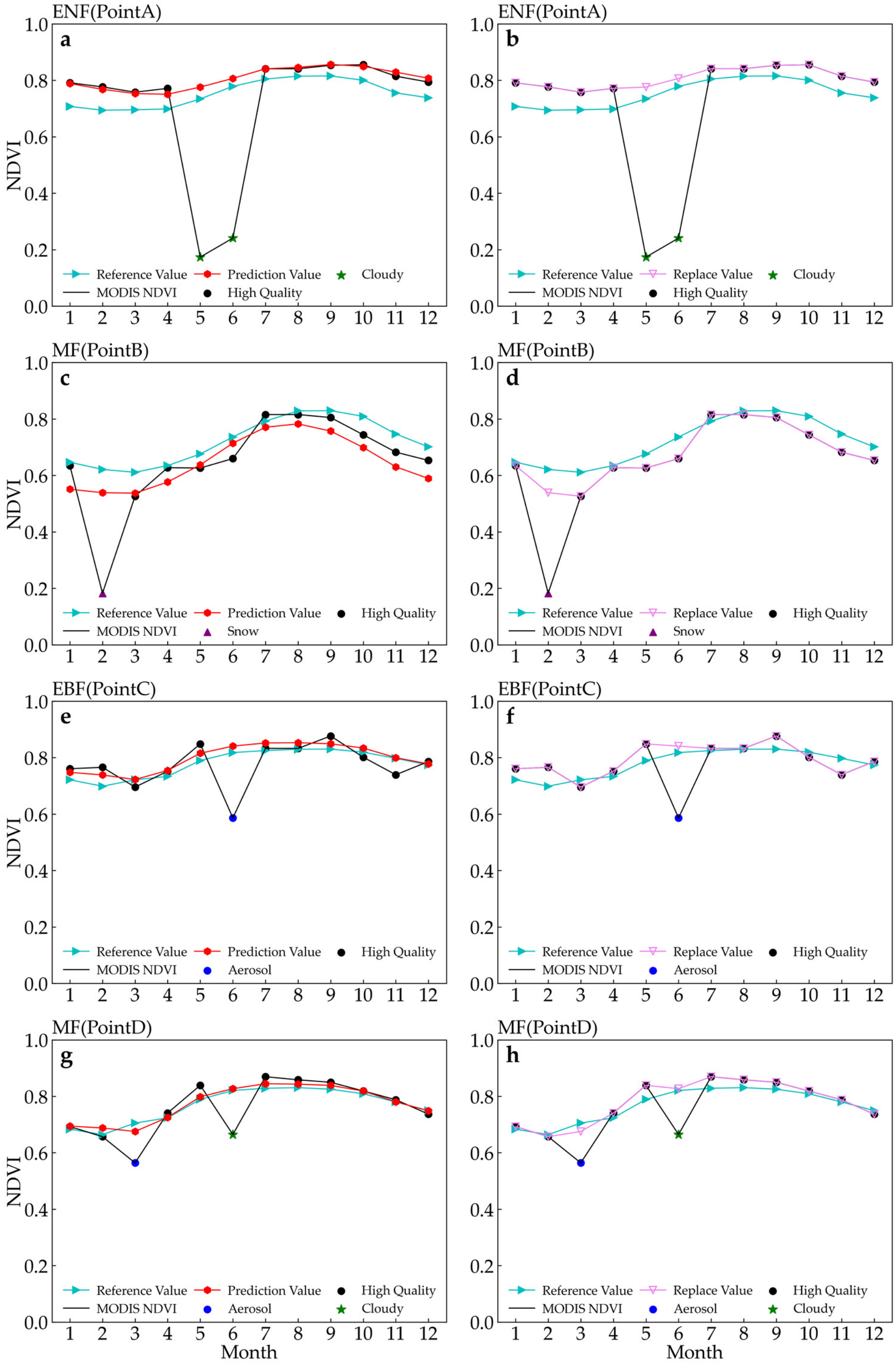

Figure 8. The comparisons between the original MODIS NDVI product and the rectified points of the estimated NDVI product affected by cloud, snow, aerosol, and mixed factors on the distinct biomes. The points affected by cloud in the evergreen needleleaf forests during 2015 are represented by (**a**,**b**); the points affected by snow in the mixed forests during the same year are represented by (**c**,**d**); the points affected by aerosol in the evergreen broadleaf forests are represented by (**e**,**f**); and the points affected by mixed factors in the mixed forests are represented by (**g**,**h**).

Figure 9 displays a comparison of different methodologies. Upon reviewing the temporal trends between 2001 and 2015, it can be inferred that the RF model and STSG are well suited for crop characteristics across two seasons and seed-sowing variations across diverse regions. Despite the ability of RF and STSG to tackle challenging topographical and climatic conditions, the LSTM model failed to account for low-lying areas and inclement weather. Consequently, the RF model exhibited greater resilience across multiple biomes.

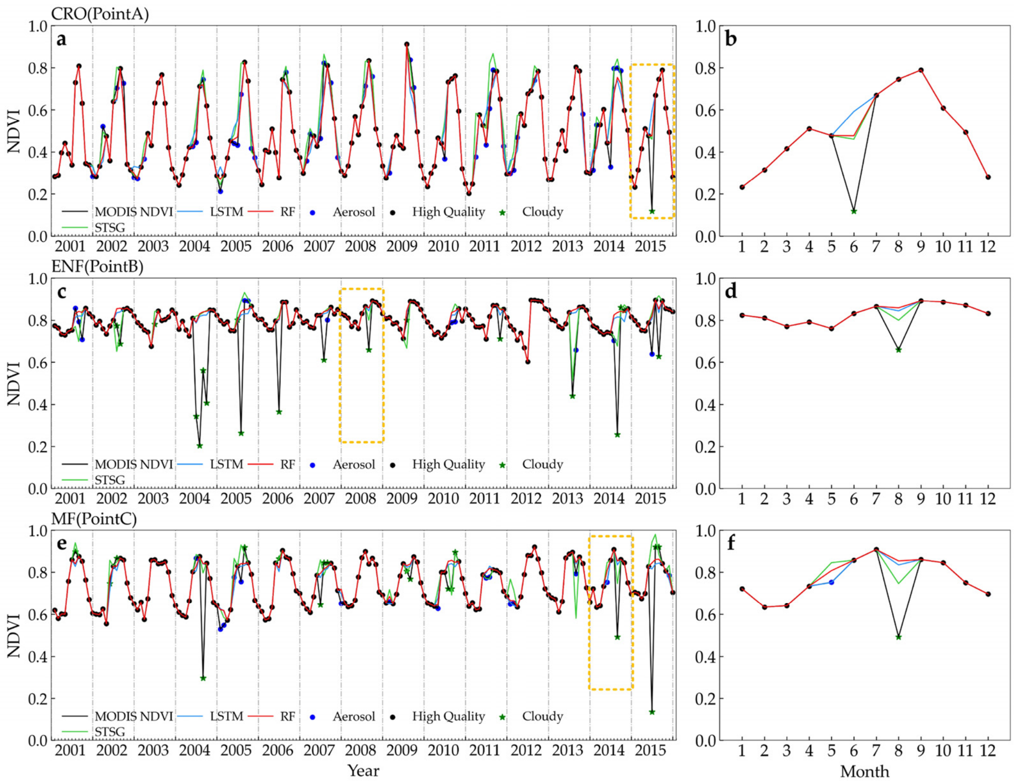

Figure 9. Three-point time series curves were estimated using various methods from 2001 to 2005. (**a**,**b**) CRO, (**c**,**d**) ENF, and (**e**,**f**) MF. The locations of the three points are depicted as a pentagon star (shown in Figure 3), and the dashed rectangle indicates the selected year (shown at (**b**,**d**,**f**)).

Figure 10 displays the MAE and RMSE of the estimated NDVI and MODIS NDVI for various land cover types on the horizontal axis, including CSL, SAV, and others. The left panels a, c, e, and g represent MAE, while the right panels b, d, f, and h represent RMSE. Blue, red, and green correspond to the STSG, LSTM, and RF methods. MODIS NDVI was chosen as the validation value of these methods based on high-quality NDVI selected via QA screening. Our findings stemmed from several factors. The random forest algorithm performs well on the MAE and RMSE of most distinct biome categories, but it could not be more effective in a few cases (Figure 10). Second, the estimated products of Figure 11 exhibited similar characteristics to those of specific biomes such as crops and forests, demonstrating greater accuracy in reflecting natural surface phenological characteristics. Thus, it is feasible for RF to estimate different terrains in different parts of China with remarkable precision. Figure 11 depicts the localized spatial distribution of the RF reconstruction product, along with the time series curves that represent the distinguishing features of a specific biome. All three methods can correct NDVI in low-quality areas to a certain extent, such as March in Anhui Province, June in the Fujian and Zhejiang provinces, and November in Chongqing. To study the characteristics of different biomes, various methodologies were evaluated based on spatial distribution data obtained from the Anhui, Fujian, Zhejiang, and Chongqing regions and their corresponding biome types, such as evergreen broadleaf forest (EBF), evergreen needleleaf forest (ENF), deciduous broadleaf forest (DBF), mixed forest (MF), and crop (CRO) (Figure 12). Using the RF method, the horizontal axis represents the boxplot of the estimated NDVI and MODIS NDVI for other months, such as January and February. The blue denotes a specific region's original observed NDVI values, including Anhui Province and Fujian Province. In contrast, the red represents the replaced values of the original low-quality NDVI using the RF estimated values of the same region. These figures provide valuable insights into various methods' performance and suitability for different categories and areas (Figure 12). A comprehensive analysis revealed that the RF model outperformed the STSG and LSTM models, as the former produced more realistic results with finer texture information. The efficacy of different approaches was further verified using growth curves, highlighting the features of different biomes.

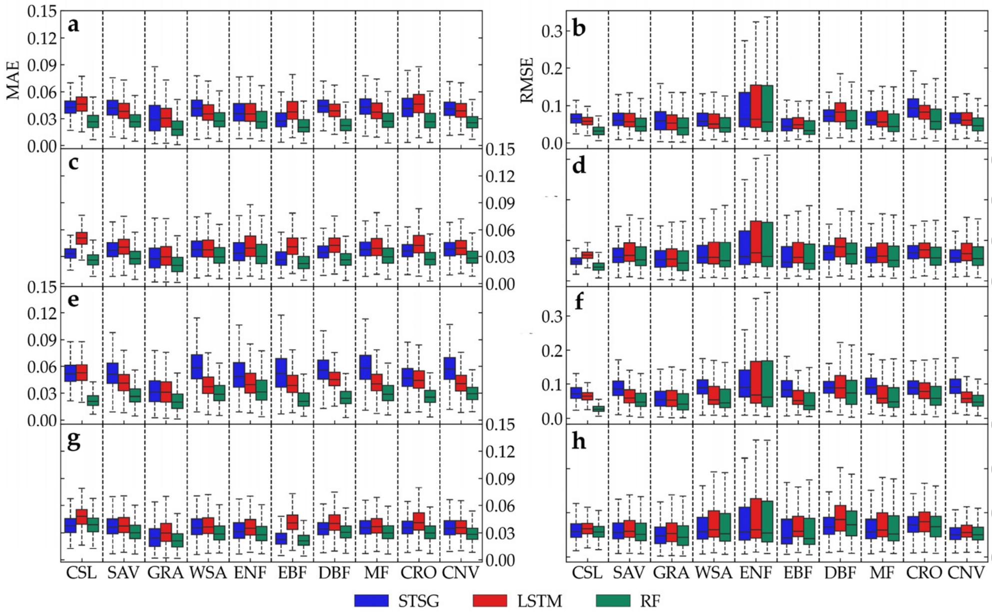

Figure 10. The comparison of different methods in different biome categories. The MAE of the estimated results for the selected years 2001, 2005, 2010, and 2015 is represented by (**a**–**d**), respectively. The RMSE of the estimated results for the same years is presented by (**e**–**h**), respectively. Note: the abbreviations of CSL, SAV, GRA, WSA, ENF, EBF, DBF, MF, CRO, and CNV stand for closed shrubland, savanna, grassland, woody savanna, evergreen needleleaf forest, evergreen broadleaf forest, deciduous broadleaf forest, mixed forest, cropland, and cropland/natural vegetation mosaic, respectively.

4.3. Model Validation

The simulated area in China was used to evaluate the accuracy of various methods for estimating NDVI against the standard NDVI in a reliable testing ground. This specific area was selected based on its low presence of low-quality pixels, which can be affected by factors such as clouds, snow, aerosols, and other possible sources of interference. The quality assessment process confirmed the determination above as being more significant. Furthermore, as approved by the QA evaluation, the simulation area also exhibited a scarcity of low-quality pixels impacted by clouds, snow, aerosols, etc. Therefore, the MODIS NDVI data obtained from this simulation area were considered to be appropriate for validation in this study.

As shown in Figure 13, the spatial pattern of the simulated NDVI was underestimated in the regions where the original high-quality NDVI was less than 0.4 and overestimated in those regions where the original NDVI was more significant than 0.4, using the STSG method. Compared with the STSG method, the estimated NDVI derived from the LSTM method differed less from the original high-quality NDVI regarding the spatial pattern, as shown in Figure 13a,b. In addition, this was also true for the histogram distribution, as seen in Figure 13f,g; however, the LSTM algorithm still yielded a problematic estimation result. As shown in Figure 13g, for the regions where the NDVI was in the range of

0.2 < NDVI < 0.4, LSTM underestimated the impact. When NDVI > 0.4, LSTM overestimated the impact. Unlike the other two algorithms, we found that the RF reconstruction method had a better overlap with the original high-quality NDVI in the statistical histogram (Figure 13h) and spatial pattern (Figure 13d). Through the separability analysis comparison, we also found that the RF reconstruction method proposed in this study outperformed the other two mainstream algorithms (shown in Table 2). Therefore, the MODIS NDVI data obtained from this simulation area were considered to be appropriate for validation in this study.

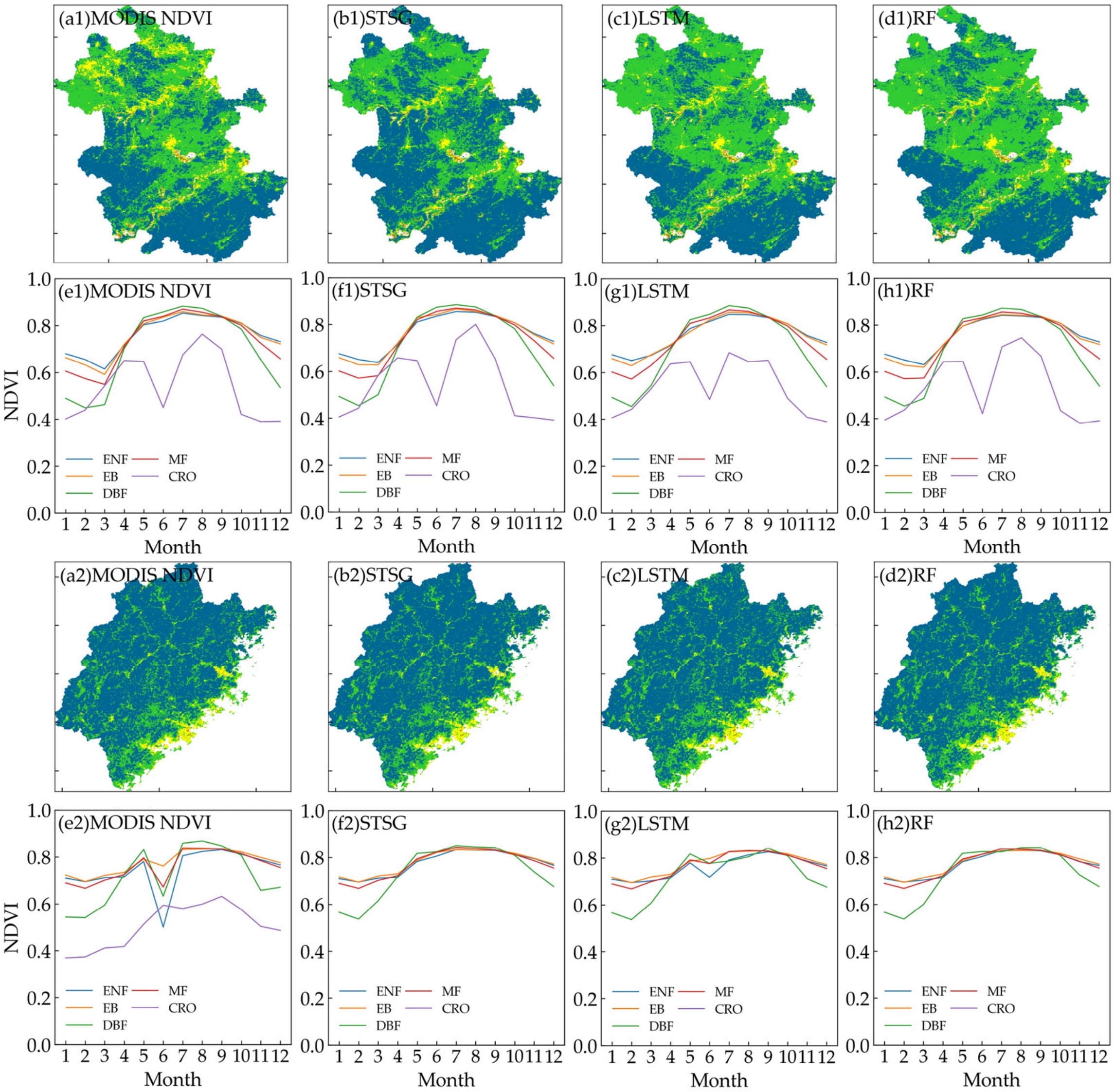

Figure 11. *Cont.*

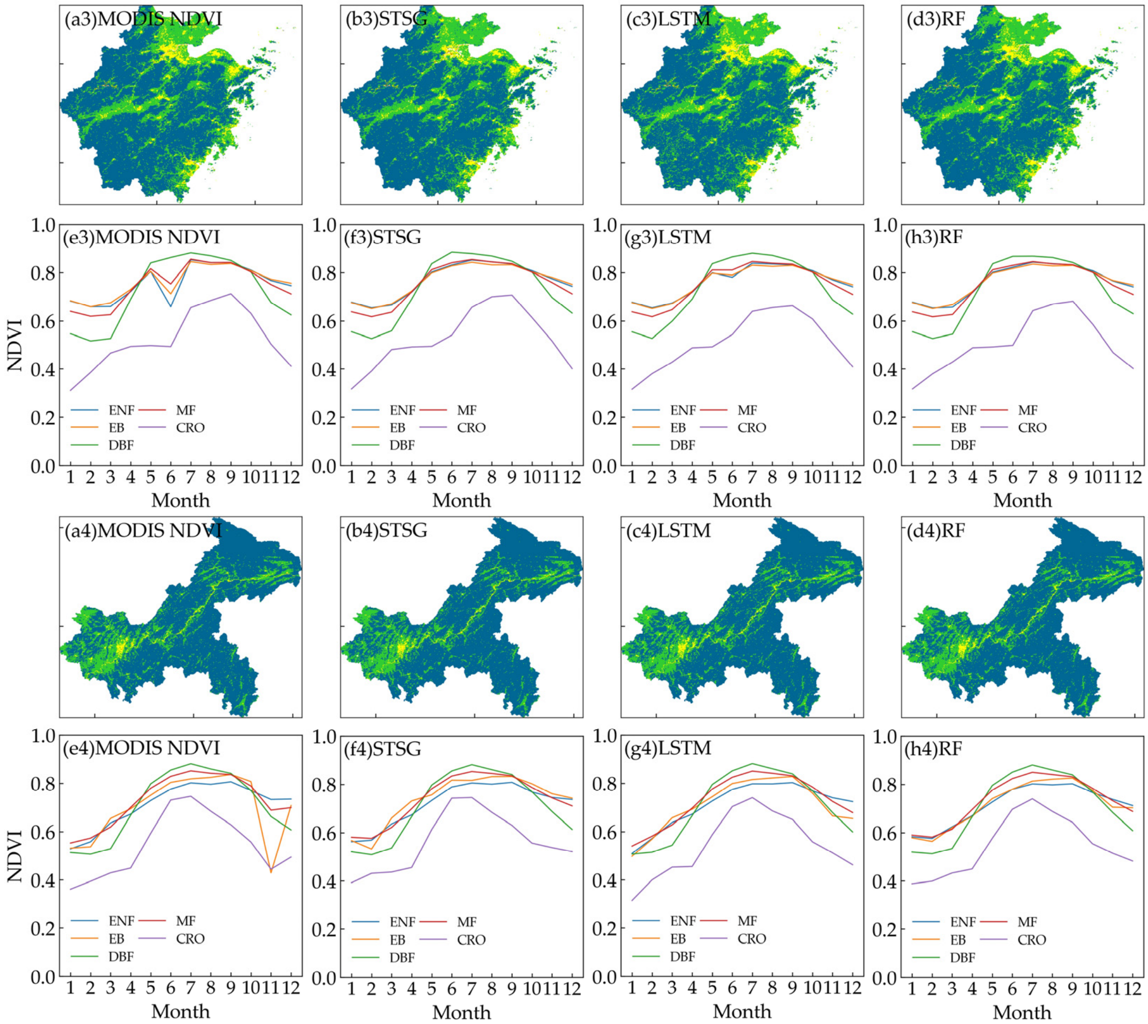

Figure 11. The reconstruction images and local spatial and phenological characteristics of specific biomes in Anhui Province, Fujian Province, Zhejiang Province, and Chongqing Province using STSG, LSTM, and RF. Note: (**a1–a4**,**e1–e4**): MODIS NDVI; (**b1–b4**,**f1–f4**): STSG; (**c1–c4**,**g1–g4**): LSTM; (**d1–d4**,**h1–h4**): RF.

As shown in Figure 14, the feasibility of the RF-based estimation result was compared with that of other models by displaying the spatial distribution and the time sequence curve of the TCA points. We found that all three methods could successfully capture the harvest condition of TCA, that is, the winter wheat is harvested in June in the TCA, and summer corn or soybeans are planted. This cultivation scheme forms a 'peak–valley–peak' pattern in the NDVI time series that reflects this condition (Figure 14e). All three methods could delineate this pattern. All three methods (i.e., LSTM, STSG, and RF) improved the contaminated NDVI from either spatial results or time sequence results (see Figure 14(b1,c1,d1,e)); however, the results of the RF-based estimates (the solid red line of Figure 14e) were closer to both the MODIS NDVI and Landsat data, with a higher consistent degree of good fitness with the data of the original high-quality areas. Compared with the LSTM and STSG methods, the RF-based process had the highest spatial congruence with the MODIS NDVI images (Figure 14(a1,d1)). We verified that the RF product accurately captured the ground's texture and actual natural land characteristics, providing higher accuracy. In other words, the RF-based model was more effective and stable in estimating low-quality NDVI areas while retaining the capacity to learn phenological information successfully.

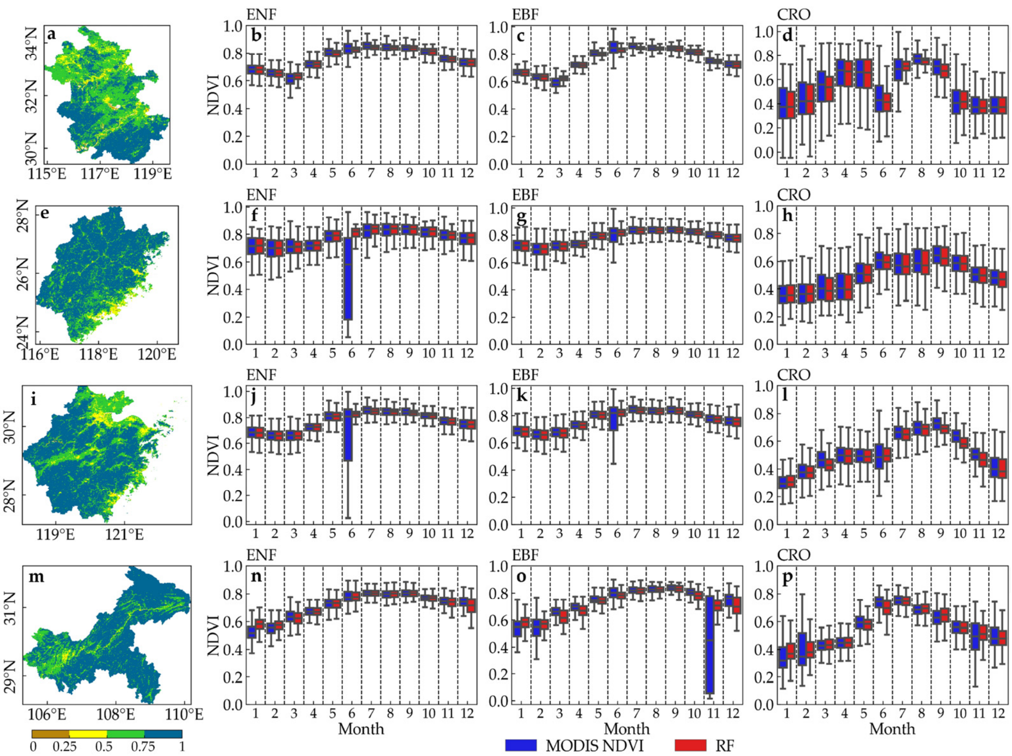

Figure 12. The spatial characteristics and phenological patterns of evergreen needleleaf forests, evergreen broadleaf forests, and croplands in Anhui Province, Fujian Province, Zhejiang Province, and Chongqing Province from 2001 to 2015 presented by (**a**–**p**).

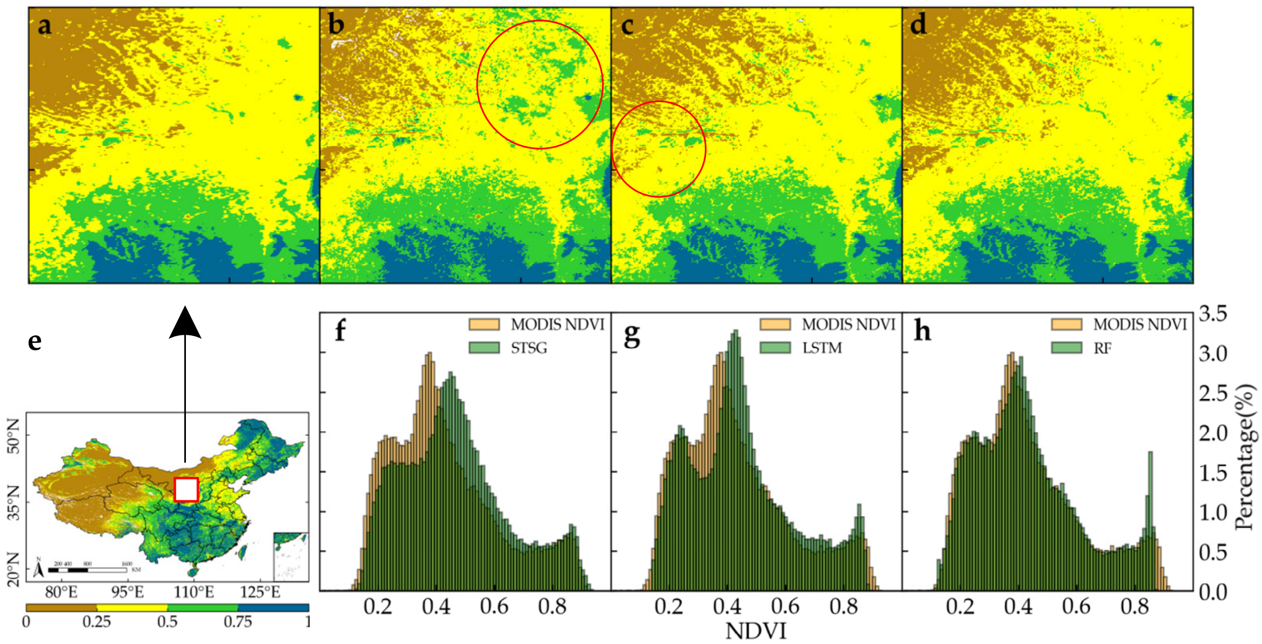

Figure 13. The simulations, the simulation performance of different methods, and the two regions marked by the red circle are other high-quality areas. (**a**) MODIS NDVI; (**b**) STSG; (**c**) LSTM; (**d**) RF; (**e**) the simulated areas of MODIS NDVI in China; (**f**) the different values of MODIS NDVI and STSG; (**g**) the different values of MODIS NDVI and LSTM; and (**h**) the different values of MODIS NDVI and RF. Note that the red circles in (**b**,**c**) denote the problematic estimated result (mainly overestimated).

Table 2. Comparisons of separability of the used methods.

	STSG	LSTM	RF
separability	0.051	0.013	0.010

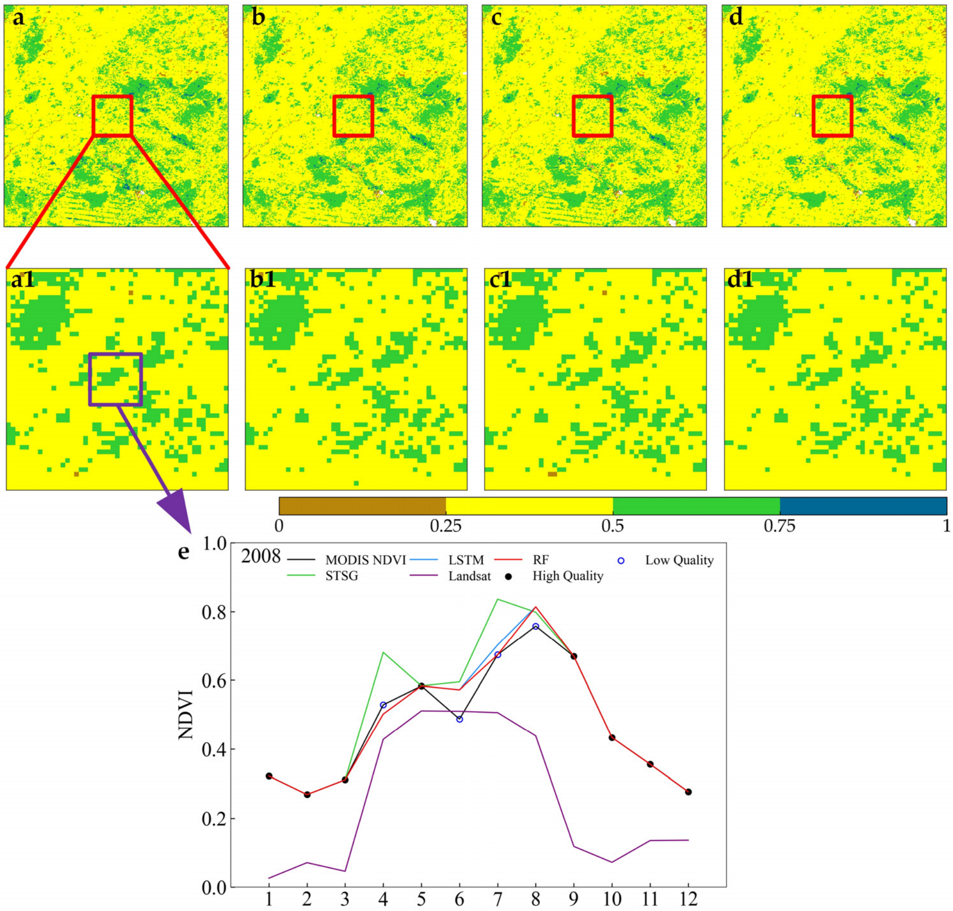

Figure 14. The comparison of different methods at the TCA site. (**a**) MODIS NDVI image (acquired June 20, 2008, for TCA), (**b**–**d**) reconstructed NDVI images using different methods: (**b**) STSG; (**c**) LSTM; and (**d**) RF (**a1**–**d1**) are enlarged views of the MODIS NDVI image, STSG simulation result, LSTM simulation result, and RF simulation result to show the spatial details, and (**e**) the time series curves of reconstructed NDVI for a small area.

This paper has proposed a novel method for reconstructing the low-quality areas of MODIS NDVI using the random forest model, specifically in the research area of China. The technique uses the relationship between MODIS NDVI products and auxiliary data, combined with long-term meteorological and geographical data, to fill in cloud-covered regions and produce a seamless spatiotemporal representation of the actual surface. The machine learning approach was tested on the complex terrain of the North China Plain using newly generated MODIS NDVI and Landsat 8 data from different sources. The product of the random forest model is closer to the actual surface representation with finer texture information than the other methods, as shown through spatial and temporal analyses. The method is also more effective at learning the phenological characteristics of typical land cover types. The results demonstrate the algorithm's universality and robustness under different climatic conditions. Overall, the random forest method outperforms the other methods in terms of accuracy and reliability in reconstructing NDVI data.

5. Discussion

It reflected the ability of the newly generated products to learn the phenological characteristics of typical ground biomes, such as evergreen needleleaf forests, evergreen broadleaf forests, deciduous needleleaf forests, deciduous broadleaf forests, mixed forests, and croplands (shown in Figures 6 and 9). Based on the results, the product is consistent with the phenological characteristics of the original high-quality area [51,52]. According to the analysis, different methods estimate the effects of varying land categories differently (shown in Figures 5 and 7). The random forest approach provided the most accurate estimation of crops, providing a basis for further research on crop yield [42,53]. The sample distribution is uniform and involves more climatic zones, which can support the model to learn enough features and produce sound learning effects for these objects.

5.1. Differences between the RF Method and Previous Methods

Compared with traditional inversion methods, such as STSG [20] and LSTM [21], RF [54] has made significant breakthroughs. Specifically, the nonlinear interactions between different factors still need to be explained to simulate them even with a state-of-the-art model, which usually results in underestimated values in these areas compared to when using a dynamic model [6]. In addition, it is challenging to identify nonlinear relationships in climate systems using linear statistical models. Moreover, the forecast targets of previous studies were not directly focused on extreme events but on the time series of rainfall anomalies. Furthermore, it took time to determine whether the extreme event had been successfully predicted, even if the expected mechanism had the same sign as the observed anomaly. Owning to the above reasons, a model that can integrate various nonlinear physical mechanisms into the model and detect weak signals that traditional linear methods can easily miss is needed. It is concluded that the RF could satisfy these requirements, and it is a high-accuracy, high-robustness, and high-interpretability model for estimating the NDVI in low-quality areas, based on the results shown in Figures 3, 13 and 14. In addition, it can thoroughly combine multiple relationships between various remote sensing products and NDVI products to achieve the project's goal in particular (shown in Figure 1), and it was established that a stable model could be developed for reconstruction. Moreover, based on the RF model, a continuous, long-term, and high-quality NDVI product could be designed after estimating NDVI values in contaminated areas. In addition, the input products had already processed the atmospheric or radiometric correction before applying the random forest algorithm, effectively avoiding uncertainties caused by error accumulation.

Based on the analysis presented in Figures 9 and 10, it can be inferred that the RF model is better suited for estimating crop characteristics across diverse terrains and regions than the LSTM model. The RF algorithm also exhibited greater resilience across multiple biomes and is effective in most cases except for a few scenarios. The TCA results depicted in Figure 14 also support the accuracy of the RF model in capturing ground texture and actual land characteristics. Moreover, the estimated products in Figure 11 demonstrate the ability of the RF model to accurately reflect the surface phenological characteristics of specific biomes such as crops and forests. Therefore, the RF model is feasible for estimating different terrains in different parts of China with remarkable precision. Finally, the reconstructed NDVI shows similar trends and patterns to the previous related works using the same data sources. Specifically, the overall upward movements of the random forest algorithm were observed, and the annual fluctuations were more noticeable, especially between 2009 and 2015 (shown in Figure 7). These fluctuations could be attributed to years of deforestation, forest protection measures, southern water irrigation, and large-scale farming soil management, where all of which have contributed to enhancing vegetation coverage. These findings of the random forest algorithm agree with those of several other research studies [55,56].

There is a significant difference in performance between these two methods in the case of the same environment. STSG requires pre-classification of MODIS NDVI time series products, which may introduce classification errors and boundary effects [23]. It requires selecting appropriate parameters, such as window size, threshold, etc., which may affect the algorithm's performance and stability. It cannot fill in missing data for multiple continuous years or seasons. LSTM is a neural network that processes data sequences and remembers values over long time intervals. It has a cell and three gates (input, output, and forget) that regulate the flow of information in and out of the cell. Moreover, it is helpful for handwriting recognition, speech recognition, machine translation, and robot control tasks.

The RF approach is better at gap restoration since it uses spatial–temporal information from all years. This applies to isolated cracks, continuous holes, and gaps in peaks and valleys. STSG can fix vegetation growth period cracks (Figure 9d) and narrow gaps (Figure 9c). Nevertheless, these do not address the gaps present during the peak growing season, as seen in Figure 9c,d and Figure 15e,k,m, or the gaps present consistently in Figure 15a,c,e,m. STSG outperforms LSTM in almost every circumstance because it uses spatial information. This supports Cao et al. [20]. However, the STSG technique is unstable at various points in the time series depicted in Figure 15b,d,f,j,l,n. The RF technique handles adverse marginal value distributions better than the others. It only eliminates somewhat unusual versions. Figure 15f,l shows that the initial time series includes marginal noise and frequent temporal fluctuations. Both figures exhibit these traits. The techniques can reduce anomalous volatility and smooth the curve if marginal data have a high negative deviation. The procedures produce this. LSTM rebuilds it in a slightly worse way. LSTM also overestimates average declines almost annually. The STSG and RF techniques best handle marginal data with low values in this context. The SG filter values may explain the STSG approach's modest oscillations, especially during the growing season. RF modelling is stable in peak and valley periods. The LSTM technique performs poorly during these periods due to excessive smoothing (Figure 15d,f,l,n). In Figure 15f, the STSG approaches reach the upper envelope of all values, while the RF approach usually only reaches the upper envelope of the best offers. This slight variation may prevent peak overestimation.

Comparing the spatial distribution and phenological characteristics of specific biomes in Yunnan Province, this section compares the results of reconstructions using the RF method and the other two methods. Figure 16 depicts the spatial distribution of the proposed RF method in July 2015, during the summer season, with extensive vegetation cover and severe cloud contamination, as evidenced by the comprehensive coverage of vegetation and cloud contamination. This is for the province of Yunnan. The RF method raises low NDVI values to high levels and achieves spatially continuous reconstruction. Figure 16a depicts the original image with high NDVI values before it was degraded by dense cloud cover. Even though LSTM can remedy low values, the results still exhibit negatively biased noise and spatial discontinuities (illustrated in Figure 16(b,b1)). The STSG procedure performs better, but the results still have some noise (Figure 16(c,c1)). Figure 16(d,d1) demonstrates that the illustrated RF method offers the best noise reduction and spatial continuity performance. Figure 16b depicts a region dominated by BNF as the date approaches the apex of BNF growth. The mean values of the original NDVI image and the three resulting images indicate that all methods increased the low NDVI values that had been corrupted. Only the proposed RF and STSG methods restored the common NDVI values to their optimum values, whereas LSTM underestimated the NDVI values (illustrated in Figure 16(b,b1)). Overall, the results demonstrate the optimal spatial performance of the RF method for maintaining critical points.

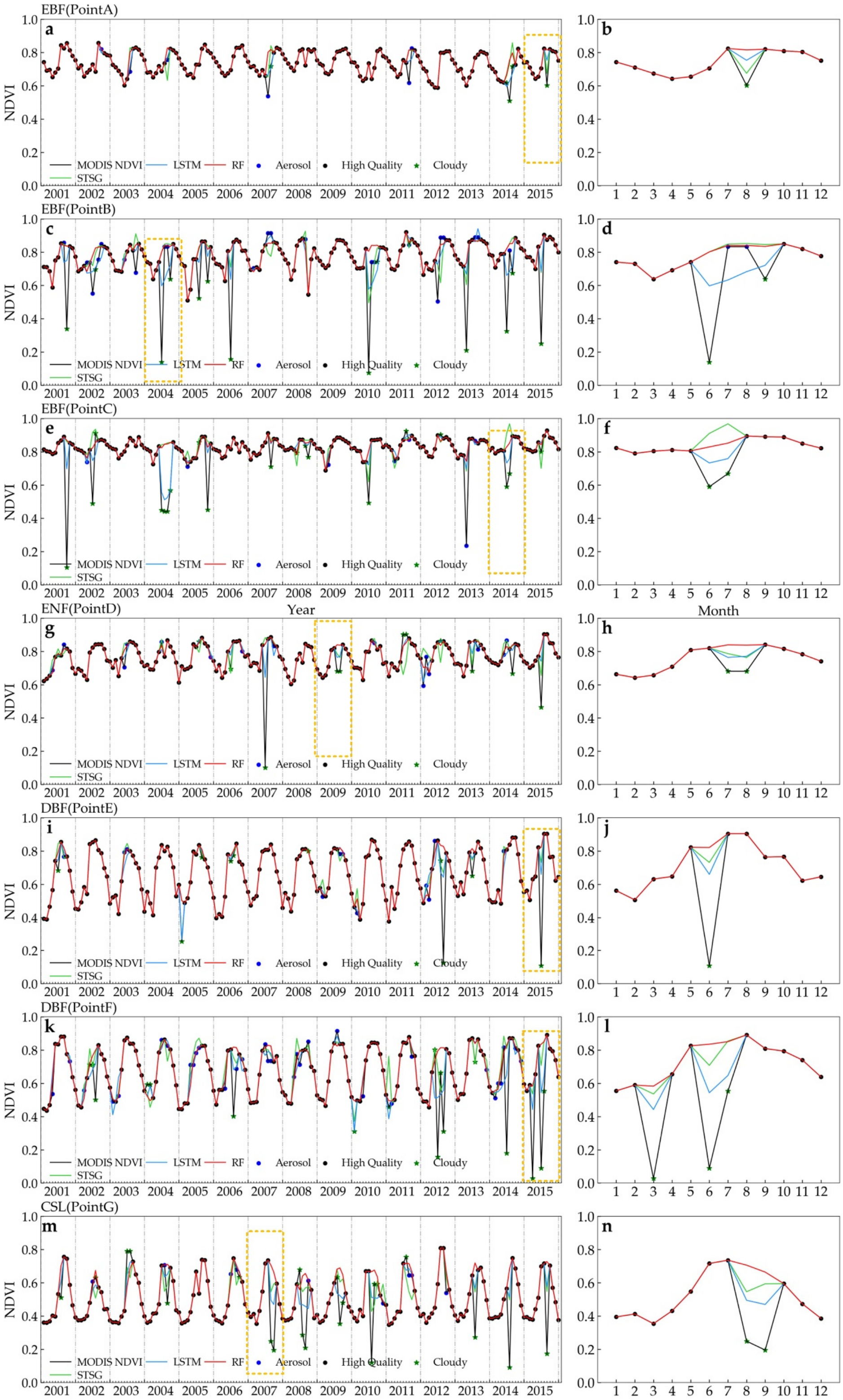

Figure 15. The performance of different methods over different vegetation types for long time series. A dashed rectangle indicates the chosen year. Note: ENF presents evergreen needleleaf forest; EBF: evergreen broadleaf forest; DBF: deciduous broadleaf forest; MF: mixed forest; CSL: closed shrubland. (**a**–**f**) EBF, (**g**,**h**) ENF, (**i**–**l**) DBF, and (**m**,**n**) CSL. The locations of the three points are depicted as a pentagon star (shown in Figure 3), and the dashed rectangle indicates the selected year (shown at (**b**,**d**,**f**,**h**,**j**,**l**,**n**)).

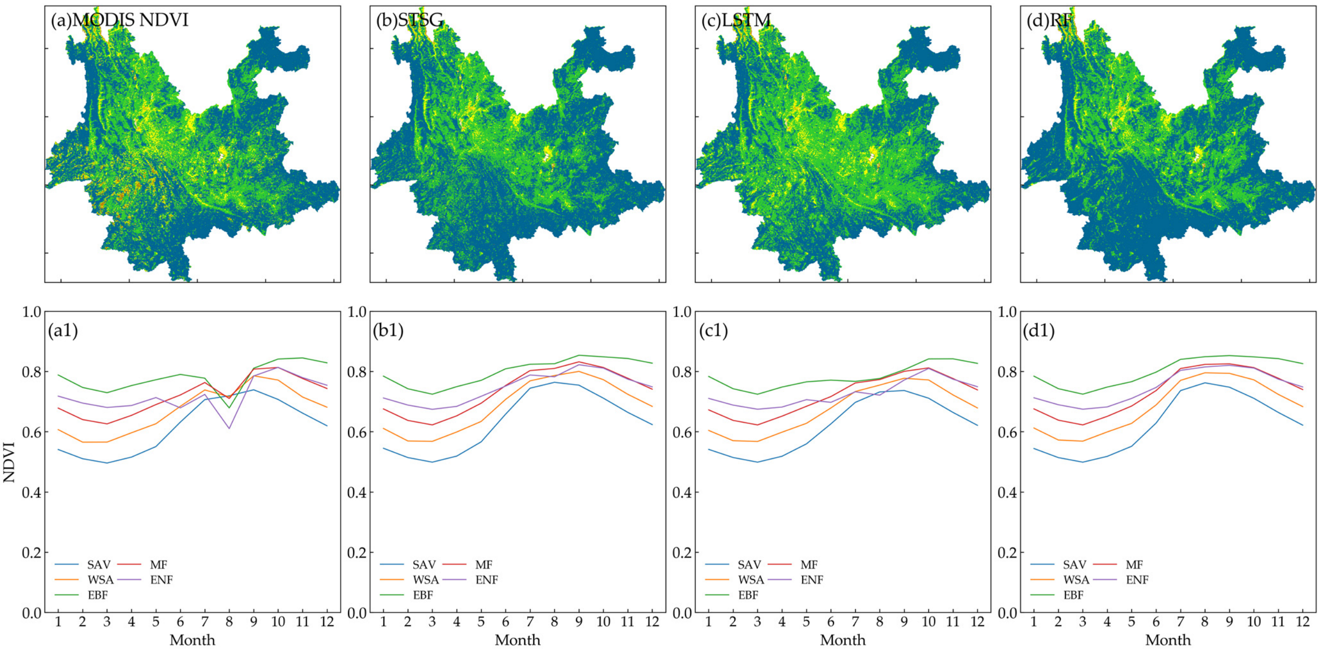

Figure 16. The reconstruction images, local spatial characteristics, and phenological characteristics of specific biomes in Yunnan Province using STSG, LSTM, and RF in July 2015. Note: (**a**,**a1**): MODIS NDVI; (**b**,**b1**): STSG; (**c**,**c1**): LSTM; and (**d**,**d1**): RF. Note: SAV, GRA, WSA, EBF, and MF are savanna, grassland, woody savanna, evergreen broadleaf, and mixed forest, respectively.

Long-time series NDVI data is widespread across various practical applications, such as vegetation monitoring, drought monitoring, land use classification, ecological assessment, climate change studies, and agricultural management. These data aid in monitoring vegetation growth, drought occurrence, and moisture status, as well as in assessing health and ecological changes. Additionally, using them facilitates the classification of land use/cover types, evaluation of ecological quality, and examination of the impacts of climate change on vegetation growth and distribution. Furthermore, long-term NDVI data enable farmers to make informed decisions regarding fertilisation and irrigation practices. The importance of NDVI data in ensuring the health and sustainability of diverse ecosystems cannot be overstated. Consequently, correcting long-time series NDVI data is of great interest, and the random forest algorithm is a valuable tool in this endeavour.

5.2. The Limitation of the RF Method

There are still some limitations to this study. First, the method may be better for MODIS sources, but the effects of other data sources require further experimentation and investigation efforts. At the same time, it only applies to China, involving smaller regions, and it may have the potential to process global products. In addition, we used default parameter values because of the large amount of experimental data and the limitations of the experimental conditions and time. Specifically, there were 125 products in this study, and it took place over 15 years. The workload was significant, requiring a multiprocessing approach to handle it. A more cost-effective algorithm is recommended in future work, and multiprocessing may be implemented to complete the process.

Moreover, the representative sample is another problem. The number and distribution of pieces are key factors affecting the learning of land features. Due to climate conditions and geographical location limitations, the model training sample needed to be sufficiently diverse in categories. It did not involve all climate zones worldwide; some regions lacked pieces to different extents. Furthermore, some land samples had fewer numbers, and some land distribution was concentrated in certain areas, such as forests, mainly in coastal areas. A few other sites may also be distributed, making characteristic learning insufficient. Thus, further exploring algorithms for sample balancing and land class identification, which will improve estimation results, is necessary.

When this method is used for estimation on a global scale, there are two problems: one is the increase in sample size; the other is that the more complex nonlinear relationship between more complex remote sensing products and NDVI requires more decisions, which will lead to an increase in the model training cycle. Therefore, in later research, multiple processes can be considered. At the same time, the data processing and model training can be run on the GPU, which has more computing cores than the CPU, which will significantly improve the computing efficiency.

6. Conclusions

Due to the nature of clouds, snow, and aerosols, they are discontinuous in space and time, severely limiting the broad application of the current NDVI products. To solve this problem, we used the random forest model to construct multisource quantitative remote sensing products such as FAPAR and LAI, as well as to find the relationship between the longitude, latitude, elevation, and other factors related to the vegetation growth process and NDVI, to avoid the influence of NDVI products alone when there continuously are multiple low-quality products. We found that when compared with the spatial–temporal Savitzky–Golay (STSG) method, our approach based on random forest (RF) methodology decreased the MAE and RMSE by 0.014 and 0.019, respectively. Compared with the long short-term memory (LSTM) method, our RF-based approach decreased the MAE and RMSE by 0.013 and 0.015, respectively. The results showed that the RF model had the best estimation performance compared to traditional linear methods such as STSG and LSTM.

Multiple verification approaches were conducted:

1. The performance of the models correcting the contaminated pixels was tested using the site-based method, which included the NDVI simulation in TCA and the actual ground observations (points A, B, and C). The results showed that the RF model had a lower MAE and RMSE than LSTM and STSG, and the correction was very close to the high-quality areas regardless of the biome type.
2. The performance of the models was tested using the time sequence test, and we found that the reconstructed NDVI had the lowest MAE and RMSE in the time series from 2001 to 2015.
3. By comparing the spatial pattern of different models, we found that the RF method could produce a product with more continuous spatial textures.

Using the RF method proposed in this study, we reconstructed a monthly NDVI product with a spatial resolution of 1 km in China from 2001 to 2015. The reconstruction product could be helpful for the yield estimation and dynamic monitoring of vegetation growth and could shed light on the processing of future cost-effective algorithms.

Author Contributions: Conceptualization, M.S., A.G. and X.Z.; formal analysis, M.S., A.G. and X.Z.; funding acquisition, X.Z.; methodology, X.Z.; writing—original draft, M.S.; writing—review and editing, M.S., A.G., X.Z., N.L., L.S. and S.Z. All authors have read and agreed to the published version of the manuscript.

Funding: This research was funded by the National Natural Science Foundation of China under grant (42090012).

Data Availability Statement: Not applicable.

Conflicts of Interest: The authors declare no conflict of interest.

References

1. Matsushita, B.; Yang, W.; Chen, J.; Onda, Y.C.; Qiu, G.Y. Sensitivity of the enhanced vegetation index (EVI) and normalised difference vegetation index (NDVI) to topographic effects: A case study in high-density cypress forest. *Sensors* **2007**, *7*, 2636–2651. [CrossRef] [PubMed]
2. Kumari, N.; Saco, P.M.; Rodriguez, J.F.; Johnstone, S.A.; Srivastava, A.; Chun, K.P.; Yetemen, O. The grass is not always greener on the other side: Seasonal reversal of vegetation greenness in aspect-driven semiarid ecosystems. *Geophys. Res. Lett.* **2020**, *47*, e2020GL088918. [CrossRef]
3. Chu, H.S.; Venevsky, S.; Wu, C.; Wang, M.H. NDVI-based vegetation dynamics and its response to climate changes at Amur-Heilongjiang River Basin from 1982 to 2015. *Sci. Total Environ.* **2019**, *650*, 2051–2062. [CrossRef] [PubMed]
4. Zhao, J.; Huang, S.Z.; Huang, Q.; Wang, H.; Leng, G.Y.; Fang, W. Time-lagged response of vegetation dynamics to climatic and teleconnection factors. *Catena* **2020**, *189*, 104474. [CrossRef]
5. Hu, T.; Myers Toman, E.; Chen, G.; Shao, G.; Zhou, Y.; Li, Y.; Zhao, K.; Feng, Y. Mapping fine-scale human disturbances in a working landscape with Landsat time series on Google Earth Engine. *ISPRS J. Photogramm. Remote Sens.* **2021**, *176*, 250–261. [CrossRef]
6. Mao, Y.J.; Van Niel, T.G.; McVicar, T.R. Reconstructing cloud-contaminated NDVI images with SAR-Optical fusion using spatio-temporal partitioning and multiple linear regression. *ISPRS J. Photogramm. Remote Sens.* **2023**, *198*, 115–139. [CrossRef]
7. Michishita, R.; Jin, Z.Y.; Chen, J.; Xu, B. Empirical comparison of noise reduction techniques for NDVI time-series based on a new measure. *ISPRS J. Photogramm. Remote Sens.* **2014**, *91*, 17–28. [CrossRef]
8. Shao, Y.; Lunetta, R.S.; Wheeler, B.; Iiames, J.S.; Campbell, J.B. An evaluation of time-series smoothing algorithms for land-cover classifications using MODIS-NDVI multi-temporal data. *Remote Sens. Environ.* **2016**, *174*, 258–265. [CrossRef]
9. Hird, J.N.; McDermid, G.J. Noise reduction of NDVI time series: An empirical comparison of selected techniques. *Remote Sens. Environ.* **2009**, *113*, 248–258. [CrossRef]
10. Chen, J.; Jönsson, P.; Tamura, M.; Gu, Z.; Matsushita, B.; Eklundh, L. A simple method for reconstructing a high-quality NDVI time-series data set based on the Savitzky–Golay filter. *Remote Sens. Environ.* **2004**, *91*, 332–344. [CrossRef]
11. Ma, M.; Veroustraete, F. Reconstructing pathfinder AVHRR land NDVI time-series data for the Northwest of China. *Adv. Space Res.* **2006**, *37*, 835–840. [CrossRef]
12. Tang, L.; Zhao, Z.M.; Tang, P.; Yang, H.J. SURE-based optimum- length S-G filter to reconstruct NDVI time series iteratively with outliers removal. *Int. J. Wavel. Multiresolut. Inf. Process.* **2020**, *18*, 2050001. [CrossRef]
13. Jonsson, P.; Eklundh, L. Seasonality extraction by function fitting to time-series of satellite sensor data. *IEEE Trans. Geosci. Remote Sens.* **2002**, *40*, 1824–1832. [CrossRef]
14. Beck, P.S.; Atzberger, C.; Høgda, K.A.; Johansen, B.; Skidmore, A.K. Improved monitoring of vegetation dynamics at very high latitudes: A new method using MODIS NDVI. *Remote Sens. Environ.* **2006**, *100*, 321–334. [CrossRef]
15. Liu, R.G.; Shang, R.; Liu, Y.; Lu, X.L. Global evaluation of gap-filling approaches for seasonal NDVI with considering vegeta-tion growth trajectory, protection of key point, noise resistance and curve stability. *Remote Sens. Environ.* **2017**, *189*, 164–179. [CrossRef]
16. Yang, Y.P.; Luo, J.C.; Huang, Q.T.; Wu, W.; Sun, Y.W. Weighted double-logistic function fitting method for reconstructing the high-quality Sentinel-2 NDVI time series data set. *Remote Sens.* **2019**, *11*, 18. [CrossRef]
17. Li, X.H.; Shen, R.P.; Chen, R.X. Improving time series reconstruction by fixing invalid values and its fidelity evaluation. *IEEE Access* **2020**, *8*, 7558–7572. [CrossRef]
18. Xu, L.L.; Li, B.L.; Yuan, Y.C.; Gao, X.Z.; Zhang, T. A temporal-spatial iteration method to reconstruct NDVI time series datasets. *Remote Sens.* **2015**, *7*, 8906–8924. [CrossRef]
19. Chu, D.; Shen, H.; Guan, X.; Chen, J.M.; Li, X.; Li, J.; Zhang, L. Long time-series NDVI reconstruction in cloud-prone regions via spatio-temporal tensor completion. *Remote Sens. Environ.* **2021**, *264*, 112632. [CrossRef]
20. Cao, R.; Chen, Y.; Shen, M.; Chen, J.; Zhou, J.; Wang, C.; Yang, W. A simple method to improve the quality of NDVI time-series data by integrating spatiotemporal information with the Savitzky-Golay filter. *Remote Sens. Environ.* **2018**, *217*, 244–257. [CrossRef]
21. Graves, A.; Graves, A. Long short-term memory. In *Supervised Sequence Labelling with Recurrent Neural Networks*; Springer: Berlin/Heidelberg, Germany, 2012; pp. 37–45.
22. Li, S.; Xu, L.; Jing, Y.H.; Yin, H.; Li, X.H.; Guan, X.B. High-quality vegetation index product generation: A review of NDVI time series reconstruction techniques. *Int. J. Appl. Earth Obs. Geoinf.* **2021**, *105*, 102640. [CrossRef]
23. Do Thi, N.; Pham, V.D.; Bui, Q.T.; Pham, V.M. Study Model for Information Reconstruction on Cloud Contaminated Area for Single Multispectral Remote Sensing Sentinel-2 Imagery using Generative Adversarial Network. *VNU J. Sci. Earth Environ. Sci.* **2022**, *38*, 32–44.
24. Liu, H.; Huang, B.; Cai, J.J. Thick Cloud Removal under Land Cover Changes Using Multisource Satellite Imagery and a Spatiotemporal Attention Network. *IEEE Trans. Geosci. Remote Sens.* **2023**, *61*, 1–18. [CrossRef]
25. Zhang, H.; Ma, J.Y.; Chen, C.; Tian, X. NDVI-Net: A fusion network for generating high-resolution normalized difference vegetation index in remote sensing. *ISPRS J. Photogramm. Remote Sens.* **2020**, *168*, 182–196. [CrossRef]
26. Li, X.Q.; Yuan, W.P.; Dong, W.J. A machine learning method for predicting vegetation indices in China. *Remote Sens.* **2021**, *13*, 1147. [CrossRef]
27. Roy, B. Optimum machine learning algorithm selection for forecasting vegetation indices: MODIS NDVI & EVI. *Remote Sens. Appl. Soc. Environ.* **2021**, *23*, 100582.

28. Padhee, S.K.; Dutta, S. Spatiotemporal reconstruction of MODIS land surface temperature with the help of GLDAS product using kernel-based nonparametric data assimilation. *J. Appl. Remote Sens.* **2020**, *14*, 18. [CrossRef]
29. Zheng, B.J.; Myint, S.W.; Thenkabail, P.S.; Aggarwal, R.M. A support vector machine to identify irrigated crop types using time-series Landsat NDVI data. *Int. J. Appl. Earth Obs. Geoinf.* **2015**, *34*, 103–112. [CrossRef]
30. Ng, M.K.; Yuan, Q.Q.; Yan, L.; Sun, J. An Adaptive Weighted Tensor Completion Method for the Recovery of Remote Sensing Images with Missing Data. *IEEE Trans. Geosci. Remote Sens.* **2017**, *55*, 3367–3381. [CrossRef]
31. Zhu, X.L.; Helmer, E.H. An automatic method for screening clouds and cloud shadows in optical satellite image time series in cloudy regions. *Remote Sens. Environ.* **2018**, *214*, 135–153. [CrossRef]
32. Malamiri, H.R.G.; Zare, H.; Rousta, I.; Olafsson, H.; Verdiguier, E.I.; Zhang, H.; Mushore, T.D. Comparison of harmonic analysis of time series (HANTS) and multi-singular spectrum analysis (M-SSA) in reconstruction of long-gap missing data in NDVI time series. *Remote Sens.* **2020**, *12*, 22.
33. Feng, Y.B.; Liu, Q.; Qu, Y.; Liang, S.L. Estimation of the Ocean Water Albedo from Remote Sensing and Meteorological Reanalysis Data. *IEEE Trans. Geosci. Remote Sens.* **2016**, *54*, 850–868. [CrossRef]
34. Yao, Y.J.; Liang, S.L.; Li, X.L.; Hong, Y.; Fisher, J.B.; Zhang, N.N.; Chen, J.Q.; Cheng, J.; Zhao, S.H.; Zhang, X.T.; et al. Bayesian multimodel estimation of global terrestrial latent heat flux from eddy covariance, meteorological, and satellite observations. *J. Geophys. Res. Atmos.* **2014**, *119*, 4521–4545. [CrossRef]
35. Xiao, Z.Q.; Liang, S.L.; Sun, R.; Wang, J.D.; Jiang, B. Estimating the fraction of absorbed photosynthetically active radiation from the MODIS data based GLASS leaf area index product. *Remote Sens. Environ.* **2015**, *171*, 105–117. [CrossRef]
36. Jia, K.; Liang, S.L.; Wei, X.Q.; Yao, Y.J.; Yang, L.Q.; Zhang, X.T.; Liu, D.Y. Validation of Global LAnd Surface Satellite (GLASS) fractional vegetation cover product from MODIS data in an agricultural region. *Remote Sens. Lett.* **2018**, *9*, 847–856. [CrossRef]
37. Yuan, W.P.; Cai, W.W.; Xia, J.Z.; Chen, J.Q.; Liu, S.G.; Dong, W.J.; Merbold, L.; Law, B.; Arain, A.; Beringer, J. Global comparison of light use efficiency models for simulating terrestrial vegetation gross primary production based on the LaThuile database. *Agric. For. Meteorol.* **2014**, *192*, 108–120. [CrossRef]
38. Xiao, Z.Q.; Liang, S.L.; Jiang, B. Evaluation of four long time-series global leaf area index products. *Agric. For. Meteorol.* **2017**, *246*, 218–230. [CrossRef]
39. Gelaro, R.; Mccarty, W.; Suárez, M.J. The modern-era retrospective analysis for research and applications, version 2 (MERRA-2). *J. Clim.* **2017**, *30*, 5419–5454. [CrossRef]
40. Simard, M.; Neumann, M.; Buckley, S. Validation of the New SRTM Digital Elevation Model (NASADEM) with ICESAT/GLAS over the United States. In Proceedings of the IEEE International Geoscience and Remote Sensing Symposium (IGARSS) 2016, Beijing, China, 10–15 July 2016; pp. 3227–3229.
41. Zamani Joharestani, M.; Cao, C.; Ni, X.; Bashir, B.; Talebiesfandarani, S. $PM_{2.5}$ prediction based on random forest, XGBoost, and deep learning using multisource remote sensing data. *Atmosphere* **2019**, *10*, 373. [CrossRef]
42. Jui, S.J.J.; Ahmed, A.M.; Bose, A.; Raj, N.; Sharma, E.; Soar, J.; Chowdhury, M.W. Spatiotemporal hybrid random forest model for tea yield prediction using satellite-derived variables. *Remote Sens.* **2022**, *14*, 805. [CrossRef]
43. Belgiu, M.; Drăguţ, L. Random forest in remote sensing: A review of applications and future directions. *ISPRS J. Photogramm. Remote Sens.* **2016**, *114*, 24–31. [CrossRef]
44. Gibson, R.; Danaher, T.; Hehir, W.; Collins, L. A remote sensing approach to mapping fire severity in south-eastern Australia using sentinel 2 and random forest. *Remote Sens. Environ.* **2020**, *240*, 111702. [CrossRef]
45. Adugna, T.; Xu, W.B.; Fan, J.L. Comparison of random forest and support vector machine classifiers for regional land cover mapping using coarse resolution FY-3C images. *Remote Sens.* **2022**, *14*, 574. [CrossRef]
46. Breiman, L. Random forests. *Mach. Learn.* **2001**, *45*, 5–32. [CrossRef]
47. Malhotra, P.; Vig, L.; Shroff, G.; Agarwal, P. Long Short Term Memory Networks for Anomaly Detection in Time Series. In Proceedings of the 23rd European Symposium on Artificial Neural Networks, Computational Intelligence and Machine Learning, ESANN 2015, Bruges, Belgium, 22–24 April 2015; p. 89.
48. Reddy, D.S.; Prasad, P.R. Prediction of vegetation dynamics using NDVI time series data and LSTM. *Model. Earth Syst. Environ.* **2018**, *4*, 409–419. [CrossRef]
49. Muruganantham, P.; Wibowo, S.; Grandhi, S.; Samrat, N.H.; Islam, N. A systematic literature review on crop yield prediction with deep learning and remote sensing. *Remote Sens.* **2022**, *14*, 1990. [CrossRef]
50. Hochreiter, S.; Schmidhuber, J. Long short-term memory. *Neural Comput.* **1997**, *9*, 1735–1780. [CrossRef]
51. Pan, S.; Zhao, X.W.; Yue, Y.J. Spatiotemporal changes of NDVI and correlation with meteorological factors in northern china from 1985–2015. In *E3S Web of Conferences 2019*; EDP Sciences: Les Ulis, France, 2019; Volume 131, p. 1040.
52. Zhao, Q.Q.; Zhang, J.P.; Zhao, T.B.; Li, J.H. Vegetation changes and its response to climate change in China Since 2000. *Plateau Meteorol.* **2021**, *40*, 292–301.
53. Li, F.; Song, G.; Liujun, Z.; Yanan, Z.; Di, L. Urban vegetation phenology analysis using high spatio-temporal NDVI time series. *Urban For. Urban Green.* **2017**, *25*, 43–57. [CrossRef]
54. Cutler, A.; Cutler, D.R.; Stevens, J.R. Random forests. In *Ensemble Machine Learning: Methods and Applications*; Springer: Berlin/Heidelberg, Germany, 2012; pp. 157–175.

55. Bryan, B.A.; Gao, L.; Ye, Y.Q.; Sun, X.F.; Connor, J.D.; Crossman, N.D.; Stafford-Smith, M.; Wu, J.G.; He, C.Y.; Yu, D.Y. China's response to a national land-system sustainability emergency. *Nature* **2018**, *559*, 193–204. [CrossRef]
56. Zastrow, M. China's tree-planting could falter in a warming world. *Nature* **2019**, *573*, 474–475. [CrossRef] [PubMed]